

Article

Two-Stage Neural Network Optimization for Robust Solar Photovoltaic Forecasting

Jinyeong Oh ¹, Dayeong So ², Jaehyeok Jo ³, Namil Kang ³, Eenjun Hwang ^{1,*}  and Jihoon Moon ^{2,3,*} ¹ School of Electrical Engineering, Korea University, Seoul 02841, Republic of Korea; wlsdud3523@korea.ac.kr² Department of ICT Convergence, Soonchunhyang University, Asan 31538, Republic of Korea; sodayeong@sch.ac.kr³ Department of AI and Big Data, Soonchunhyang University, Asan 31538, Republic of Korea; ajdad123@sch.ac.kr (J.J.); vkdnjtmxk999@sch.ac.kr (N.K.)

* Correspondence: ehwang04@korea.ac.kr (E.H.); jmoon22@sch.ac.kr (J.M.)

Abstract: Neural networks (NNs) have shown outstanding performance in solar photovoltaic (PV) power forecasting due to their ability to effectively learn unstable environmental variables and their complex interactions. However, NNs are limited in their practical industrial application in the energy sector because the optimization of the model structure or hyperparameters is a complex and time-consuming task. This paper proposes a two-stage NN optimization method for robust solar PV power forecasting. First, the solar PV power dataset is divided into training and test sets. In the training set, several NN models with different numbers of hidden layers are constructed, and Optuna is applied to select the optimal hyperparameter values for each model. Next, the optimized NN models for each layer are used to generate estimation and prediction values with fivefold cross-validation on the training and test sets, respectively. Finally, a random forest is used to learn the estimation values, and the prediction values from the test set are used as input to predict the final solar PV power. As a result of experiments in the Incheon area, the proposed method is not only easy to model but also outperforms several forecasting models. As a case in point, with the New-Incheon Sonae dataset—one of three from various Incheon locations—the proposed method achieved an average mean absolute error (MAE) of 149.53 kW and root mean squared error (RMSE) of 202.00 kW. These figures significantly outperform the benchmarks of attention mechanism-based deep learning models, with average scores of 169.87 kW for MAE and 232.55 kW for RMSE, signaling an advance that is expected to make a significant contribution to South Korea's energy industry.

Keywords: renewable energy analysis; solar photovoltaic forecasting; neural network optimization; Optuna; online learning; multistep-ahead prediction; random forest



Citation: Oh, J.; So, D.; Jo, J.; Kang, N.; Hwang, E.; Moon, J. Two-Stage Neural Network Optimization for Robust Solar Photovoltaic Forecasting. *Electronics* **2024**, *13*, 1659. <https://doi.org/10.3390/electronics13091659>

Academic Editors: Catalina Rus-Casas, Francisco José Muñoz-Rodríguez, Gabino Jiménez Castillo and Domenico Mazzeo

Received: 5 March 2024

Revised: 11 April 2024

Accepted: 23 April 2024

Published: 25 April 2024



Copyright: © 2024 by the authors. Licensee MDPI, Basel, Switzerland. This article is an open access article distributed under the terms and conditions of the Creative Commons Attribution (CC BY) license (<https://creativecommons.org/licenses/by/4.0/>).

1. Introduction

Global climate change and sustainable development are two of the most pressing issues related to energy production and are receiving a great deal of attention around the world [1]. While energy consumption continues to grow, most energy production still relies on fossil fuels, including natural gas, coal, and oil [2]. The excessive use of these fuels is increasing greenhouse gas (GHG) emissions and causing climate anomalies around the world [3]. If our reliance on fossil fuels continues, GHG emissions are expected to increase by 30% over the next 20 years, increasing the potential for energy crises and environmental risks [4]. In response to these challenges, researchers and governments are intensifying their exploration of renewable energy resources [5]. Given the high rate of GHG emissions, renewable energy is considered a viable alternative for future energy management [4,5]. The use of renewable energy sources such as solar, wind, and biomass is considered a sustainable solution from an environmental perspective [1,2].

Due to its non-polluting and sustainable/renewable characteristics, photovoltaic (PV) energy has received considerable attention as a solution to climate change, efficiently

producing energy through the harmonious operation of its main components, as shown in Table 1 [6]. In this context, solar PV power generation is an innovative technology that directly converts the energy of sunlight into electricity [7]. It is based on the principle of converting the flow of electrons generated by solar panels through the photoelectric effect into electric current, and this direct current needs to be converted into alternating current that can be used in our daily lives [6,7]. In addition, solar PV power generation has the advantage of being easy to install, having infinite resources, being environmentally friendly, and being able to generate electricity without noise or pollutant emissions compared to other renewable energy sources [8]. Because of these characteristics, the proportion of solar PV generation and use is expected to continue to increase in the future [7,8].

Table 1. Key components and functions of the solar photovoltaic (PV) system.

Component	Function
Solar cell panel	The core component that converts sunlight into electrical energy
Inverter	Converts direct current (DC) into alternating current (AC) that can be used
Battery	Stores electricity
Charge controller	Controls the flow of electricity to prevent battery overcharging
Wiring	Connects the components of the system

Predicting solar PV power generation is very important for the operation of a sustainable energy system, including maintaining a balance between energy production and consumption and optimal utilization of energy resources [9]. However, compared to traditional energy sources, the dependence of solar PV power generation on environmental factors (e.g., sensitivity to changes in weather conditions) introduces significant variability. This variability, coupled with the dynamic nature of these environmental influences over time, makes the task of accurately predicting solar PV power generation extremely challenging [8,9]. For a complete understanding of the terms and acronyms used in this context, please refer to Appendix A, which provides definitions for key acronyms and variables discussed herein. From the perspective of technological progress, solar PV power generation forecasting has evolved significantly over time [10,11].

Initially, traditional forecasting methods such as simple statistical and physical models were widely used. While effective at capturing linear relationships, these methods were often inadequate for modeling the complex, nonlinear patterns that characterize solar energy production [11]. Subsequently, with the gradual introduction of machine learning (ML) techniques, the ability to learn and predict complex data patterns has improved. For example, advances in ML and the subsequent integration of deep learning (DL) algorithms have significantly surpassed the capabilities of traditional forecasting methods, enabling more accurate and reliable predictions. These advances have played a key role in improving the accuracy of solar PV power generation forecasting, thereby contributing to more effective energy management and stable operation of the power grid [12–19].

Qazi et al. [12] developed an artificial neural network (ANN)-based solar irradiance prediction method based on weather data analysis. Wang et al. [13] proposed a forecasting scheme using nonlinear time series analysis to predict solar power in smart grids. Van der Meer et al. [14] used two computational methods, autoregressive integrated moving average (ARIMA) models and mixed integer linear programming, for PV power forecasting and optimal electric vehicle (EV) charging management, respectively. Voyant et al. [15] developed and compared several ML algorithms, such as nearest neighbor and bootstrap aggregation, to accurately predict solar irradiation. Almonacid et al. [16] used ANNs to demonstrate prediction performance metrics of concentrator PV technology. Wang et al. [17] proposed two ML methods based on support vector machine (SVM) and adaptive learning to predict solar irradiance with high accuracy. Zhang et al. [18] developed a Bayesian network-based prediction scheme to perform spatio-temporal analysis for advanced short-term prediction of PV power generation. Al-Dahidi et al. [19] proposed a day-ahead

solar PV power generation prediction method based on an ensemble of diversified ANNs optimized with bagging and bootstrapping techniques.

In particular, DL models have received much attention due to their structure and learning method, which are excellent for processing data with complex patterns [20–25]. Abdel-Nasser and Mahmoud [20] developed a PV power prediction model using deep long short-term memory (LSTM) networks, which captures temporal dynamics with high accuracy. Patel [21] proposed a solar irradiance prediction based on the exploration of LSTM and convolutional neural networks (CNNs) to overcome the challenges of model convergence and accuracy. Wen et al. [22] developed a novel multistep-ahead prediction scheme for PV power rate control using deep CNNs and stacked sky images, bypassing the need for additional time series models and exogenous variables for industrial suitability. Jiao et al. [23] proposed a novel DL architecture for solar irradiance prediction that integrates convolutional graph neural networks with LSTM to improve accuracy and reliability for distributed PV systems. Zameer et al. [24] proposed two DL models based on bidirectional LSTM (Bi-LSTM) and gated recurrent unit (GRU) to achieve superiority in short-term solar PV prediction over traditional methods such as lasso, ridge, elastic net, and SVM, highlighting the robustness and precision of DL. Rocha et al. [25] conducted an in-depth analysis using LSTM, Bi-LSTM, and temporal convolutional network (TCN) for predicting solar PV generation on a 1320 watt-peak (Wp) amorphous plant, demonstrating the superior performance of TCN in terms of accuracy for both short-term (15-minute) and long-term (24-h) predictions.

However, the reliability of current solar PV power generation forecasting is often compromised by several factors, leading to inaccuracies. The application of advanced DL techniques as baseline models is often hampered by the need for high-performance computing resources, such as graphics processing units (GPUs) [26]. In addition, the practicality of implementing such advanced models is further limited in environments where energy managers may find the complexity of ML and DL daunting, and where energy companies or government agencies do not always have the budget or infrastructure to support high-end computing resources. DL techniques require the management of multiple hyperparameters, which adds complexity to the optimization process and can hinder model learning [27]. This complexity may limit practical applications in the energy sector, where DL expertise is not widely available. Identifying the optimal configuration of neural networks (NNs), such as the appropriate number of hidden layers, is a significant challenge and research gap that affects prediction accuracy [27,28]. Simply increasing the number of hidden layers does not guarantee improved model performance [28], and what works in one scenario may not be effective in another [29]. Consequently, researchers have attempted to improve prediction performance by integrating multiple deep neural network (DNN) models with different numbers of hidden layers, a strategy that merits further exploration [29]. In the face of these challenges, stacking ensemble learning emerges as a powerful solution that is particularly adept at overcoming the twin challenges of technical complexity and resource constraints [29–32].

Bâra and Oprea [30] incorporated weather forecast errors into the forecasting method for various PV systems, including grid-tied, hybrid, and off-grid setups. This study demonstrated that stacking ensemble learning could adjust PV forecasts based on these errors, leading to significant improvements in forecast accuracy across different PV system sizes and connectivity. Another investigation [31] proposed a stacking ensemble learning method that combines ML algorithms such as random forest (RF) and extreme gradient boosting with DL techniques such as DNNs and GRUs. This approach used weather data and system performance to predict PV generation for both on-grid and off-grid systems and showed that incorporating battery load and state of charge significantly improved the model's ability to accurately estimate potential power output. Further exploration [32] developed a stacking ensemble learning method that integrates deterministic and stochastic models to address the complexity of PV system forecasting. This method proved to be particularly effective in reducing error rates and improving forecast reliability for various

PV system types, demonstrating the ability of stacking ensemble learning to mitigate the limitations of individual forecasting models.

In addition, the effectiveness of traditional time-series forecasting models tends to decrease with the time since the last training, indicating the need for innovative approaches such as online learning [33]. To overcome these problems, we propose a novel online learning-based solar PV power generation forecasting model using two-stage NN optimization. This model aims to facilitate accurate and fast multistep-ahead forecasting in computing environments without GPU support, with a focus on Incheon's smart city development [34]. This study raises important research questions regarding the effectiveness of stacking ensemble models in improving prediction accuracy and their performance in environments with limited computing resources. The proposed method addresses key issues and makes a significant contribution to the field with an online learning-based prediction model that improves both accuracy and computational efficiency, as detailed in the main contributions of this paper:

- We use Optuna for hyperparameter optimization within scikit-learn's MLPRegressor and implement fivefold cross-validation to ensure DNN model development with sufficient training data, even on low-performance systems.
- We develop an online learning approach for the meta-regression model using a Ranger-based RF model, which ensures accurate predictions over time despite the increasing gap between training and evaluation periods.
- By interpreting variable importance from the RF, we highlight the contributions of specific DNN models, enhancing the practical understanding for energy managers and the applicability of the proposed method.
- We demonstrate the superiority of the proposed method through 11-point multistep-ahead forecasting, minimizing uncertainty and outperforming various statistical and DL models in mean absolute error (MAE) and root mean square error (RMSE).

The remainder of this paper is organized as follows. Section 2 introduces the dataset composition and preprocessing, as well as the methodology and experimental setup. Section 3 presents the results of the experiments, which demonstrate the effectiveness of the proposed method. Section 4 discusses the limitations of the study and future directions. Finally, Section 5 summarizes the main results and contributions of the work.

2. Materials and Methods

2.1. Dataset Description

2.1.1. Dataset Collection

Incheon [35], also known as Incheon Metropolitan City, is a major international metropolis in South Korea that has established itself as a pioneer in global exchange and creative urban planning ideas. Since opening as an international port in 1883, Incheon has grown into a world-class city with a population of more than three million people. Connected to various parts of the world through places such as Incheon International Airport and Incheon Port, Incheon serves as a transportation hub in Northeast Asia. Incheon also hosted the 2014 Asian Games and is known as a smart city. The city, along with Seoul and Busan, received a high rating in the 2022 Smart City Index released [36]. This rating shows how much Incheon cares about smart city management and infrastructure services. In particular, Incheon is making efforts to actively utilize new and renewable energy, especially solar power generation [37].

Therefore, we used solar PV power generation data from the Incheon area located on the west coast of South Korea in this study. We also decided to use the solar PV power generation dataset from Incheon for the following reasons: First, Incheon's location on the west coast of South Korea makes it the perfect place for high solar irradiance and relatively stable sunshine, especially in the summer. Second, Incheon has a temperate climate, with cold, dry winters and hot, humid summers, so a wide range of seasonal variations can be taken into account when analyzing and optimizing the performance of solar PV systems. In addition, Incheon's strong commitment to renewable energy and smart city implementation

ensures excellent reliability in terms of data quality and coverage. This is essential for this study into the benefits of solar energy and its function in smart cities.

In this paper, we used solar PV power generation data collected from three solar power plants in Incheon: New-Incheon Sonae, New-Incheon Observatory, and Incheon Fishery Water Purification Plant. These data are publicly available data collected through the Korea Public Data Portal [38] and were collected at 11 data points per day from 8:00 a.m. to 6:00 p.m. at hourly intervals from 1 January 2018, to 31 December 2019. We divided the data in a 5:5 ratio from 1 January 2018, to 31 December 2018, as the training set and from 1 January 2019, to 31 December 2019, as the test set. Table 2 shows the statistical analysis of the data collected from each location.

Table 2. Statistical insights and parameters of Incheon’s solar PV installations (unit: kW).

Statistics	New-Incheon Sonae		New-Incheon Observatory		Incheon Fishery Water Purification Plant	
	Training Set	Test Set	Training Set	Test Set	Training Set	Test Set
Mean	317.26	286.56	309.96	295.22	330.91	323.40
Standard error	3.72	3.89	3.70	3.49	4.01	3.82
Median	286.25	232.50	285.88	264.52	296.75	288.00
Mode	0	0	0	0	0	0
Standard deviation	235.67	246.43	234.24	221.27	254.25	242.36
Variance	55,538.34	60,727.81	54,867.24	48,958.34	64,645.42	58,737.13
Kurtosis	−1.10	−1.01	−1.21	−1.11	−1.10	−1.08
Skewness	0.31	0.52	0.28	0.35	0.34	0.36
Range	927.93	889.00	849.37	797.01	970.87	904.79
Minimum	0	0	0	0	0	0
Maximum	927.93	889.00	849.37	797.01	970.87	904.79
Sum	1,273,793.95	1,150,536.24	1,244,471.64	1,185,312.06	1,328,589.98	1,298,457.14
Number of observations	4015	4015	4015	4015	4015	4015
Location	Namdong-gu, Incheon		Seo-gu, Incheon		Seo-gu, Incheon	
Capacity (MW)	0.998		0.200		1.742	
Year of completion	Nov. '11		Sep. '12		Dec. '17	
Remarks	RPA		RPS		RPS	

MW, megawatt; RPA, Renewable Portfolio Standard Act (assumed context based on the content); RPS, Renewable Portfolio Standard.

The Incheon Fishery Water Purification Plant appears to have the most efficient PV system of the three, based on data showing that it has the highest average solar energy output throughout the training and test sets. The New-Incheon Sonae, on the other hand, shows reduced energy output, with a significant drop in the test set, suggesting possible unpredictability or seasonal effects on performance. Nevertheless, the energy production statistics appear to be fairly evenly distributed with minimal fluctuations, as indicated by the observed kurtosis and skewness across all installations, indicating stable operating conditions.

2.1.2. Dataset Preprocessing

In order to construct a forecasting model using collected data, it is essential to consider various external variables that have a significant impact on solar PV power generation. In this paper, we considered time stamps and weather information as input variables to develop a robust solar PV power generation forecasting model. These factors are very important because they directly affect the efficiency and performance of solar PV systems, and they are variables that can be realistically considered in real industrial applications in South Korea [39].

Time data consists of month, day, and hour data. Time data are a one-dimensional form of data, that can be challenging to use because it is difficult to accurately reflect its periodicity. For example, 30 November and 1 December are actually adjacent dates and times, but in the one-dimensional form of day data, there is a numerical difference of 29. In this paper, we applied Equations (1)–(4) to augment the one-dimensional month and

day data with continuous data in two-dimensional space to reflect the periodicity of the data [39,40].

$$Month_X = \sin(360^\circ / 12 \times Month), \quad (1)$$

$$Month_Y = \cos(360^\circ / 12 \times Month), \quad (2)$$

$$Day_X = \sin(360^\circ / LDM_{Month} \times Day), \quad (3)$$

$$Day_Y = \cos(360^\circ / LDM_{Month} \times Day), \quad (4)$$

where LDM_{Month} refers to the last day of the month to which a given day belongs. For example, if it is June, the LDM_{Month} is 30. If it is July, the LDM_{Month} is 31. This information is useful for determining what month a given day belongs to and how many days are in that month.

However, for the time period from sunset to sunrise, 0 is recorded regardless of any weather value. Therefore, this study considered the time period from 8:00 a.m. to 6:00 p.m. It is difficult to reflect the periodicity when reduced to 11 variables (8–18) and converted into two dimensions; therefore, 11 variables were generated by one-hot encoding.

The weather data essential for this study, especially for the prediction of solar PV power generation at three locations in Incheon, were obtained from the Incheon Meteorological Station, located at 37.47772 latitude and 126.6249 longitude, operated by the Korea Meteorological Administration (KMA). These data, which are critical to the input variables in DNN models, were obtained from the Weather Data Service's Meteorological Data Portal [41]. The KMA provides different types of weather forecasts, such as ultra-short-term forecasts, short-term forecasts, medium-term forecasts, and long-term forecasts. The ultra-short-term forecast predicts weather elements such as temperature, precipitation, and lightning strikes at one-hour intervals for up to four hours ahead, providing instant weather insights, while the short-term forecast extends predictions for variables such as temperature, humidity, wind speed, and precipitation up to three days ahead, with updates every three hours [42].

Since a solar PV power generation forecasting model needs to have forecasts at least one day ahead for effective power utilization planning [43], we specifically used daily average temperature, daily minimum temperature, daily maximum temperature, air temperature, humidity, wind speed, and precipitation data from the KMA short-term forecast [39]. Although the forecasts are available three days in advance, for the purpose of this study, we only focus on using the forecasts provided one day in advance to improve the accuracy and reliability of the day-ahead forecasts. The solar PV power generation data, which are collected in 1-h increments, contrast with the KMA short-term forecast data, which are initially available in 3-h increments. For these purposes, these data have been cleverly converted to hourly intervals using linear interpolation, which improves the temporal resolution and applicability for solar PV power forecasting.

A key challenge for KMA short-term forecasts is the lack of solar irradiance data, which are critical for predicting solar PV power generation. To address this, we adopted a creative strategy to indirectly simulate the effects of solar irradiance on the proposed method. By examining how solar power generation changes with different weather conditions, such as season and time of day, we could estimate the role of solar irradiance in power generation. In addition, to compensate for the lack of direct solar irradiance data and to improve the predictive accuracy of our model, we developed multiple DNN models and applied the stacking ensemble method. This innovative two-step strategy enhances the ability of our model to mimic the effects of solar irradiance and significantly improves the prediction accuracy. As a result, this approach allowed us to build a comprehensive model with 22 carefully selected input variables, as shown in Table 3.

Table 3. Input variables for solar PV power generation forecasting modeling.

No.	Input Variable	Variable Type	No.	Input Variable	Variable Type
1	$Month_X$	Numeric	12	3:00 p.m.	Binary
2	$Month_Y$	Numeric	13	4:00 p.m.	Binary
3	Day_X	Numeric	14	5:00 p.m.	Binary
4	Day_Y	Numeric	15	6:00 p.m.	Binary
5	8:00 a.m.	Binary	16	Avg. Temperature	Numeric
6	9:00 a.m.	Binary	17	Min. Temperature	Numeric
7	10:00 a.m.	Binary	18	Max. Temperature	Numeric
8	11:00 a.m.	Binary	19	Temperature	Numeric
9	12:00 p.m.	Binary	20	Humidity	Numeric
10	1:00 p.m.	Binary	21	Wind Speed	Numeric
11	2:00 p.m.	Binary	22	Precipitation	Numeric

Our dataset includes only external variables, such as weather conditions and time stamps, and intentionally omits internal factors. This choice ensures that the dataset is broadly applicable across South Korea, without being limited by the specific details of individual solar PV systems. This universal applicability is key to developing effective energy harvesting strategies that can be easily adapted to different solar PV installations in South Korea. Thus, the dataset configuration can provide great value by supporting the creation of predictive models that are both powerful and widely applicable, helping power producers improve their operations and increase the environmental friendliness of their power generation.

Min–max normalization can make all input variables similar by putting them on a scale from 0 to 1 [44]. This technique allows the model to learn more accurately and overcome any shortcomings in the data. We used Equation (5) to train the consistency of the DL-based solar PV power generation prediction model by applying min–max normalization to all input variables, including time stamps and weather information.

$$X_{Norm} = (X - X_{Min}) / (X_{Max} - X_{Min}), \quad (5)$$

where X_{Norm} represents the new value of a number in the set of observations X after normalization. The minimum and maximum values of X are represented by the variables X_{Min} and X_{Max} . We applied them to the training set before applying the X_{Norm} values from the training set to the test set. As a result, the minimum and maximum values of an input variable can be zero and one.

Figure 1 shows a synchronized overview of normalized meteorological variables and solar PV power generation at three different locations in Incheon for July 2019. Each variable—temperature, humidity, wind speed, precipitation, and PV power generation for three solar power plants in Incheon—is represented by a min–max normalization to ensure an equitable scale of 0 to 1. This normalization technique allows us to identify patterns and correlations in the fluctuating climate of Incheon’s monsoon season and its subsequent impact on PV power generation. The hourly time index represents a sequential timeline that captures the intricacies of solar energy variability in a region characterized by strong climatic transitions. This graphical representation not only illustrates the temporal distribution of each parameter but also serves as a powerful visual reinforcement of the variability inherent in solar energy systems, especially during periods of climatic extremes such as the onset of the East Asian Monsoon [45].

We ensured that the processed datasets were designed to enhance replicability and further research. To this end, the preprocessed datasets are publicly available for those who wish to use them in model training or additional studies. Researchers can find these datasets in the Supplementary Material of this paper, specifically in Tables S1–S3. This step is taken to underscore our commitment to openness and the advancement of scientific inquiry in the energy field.

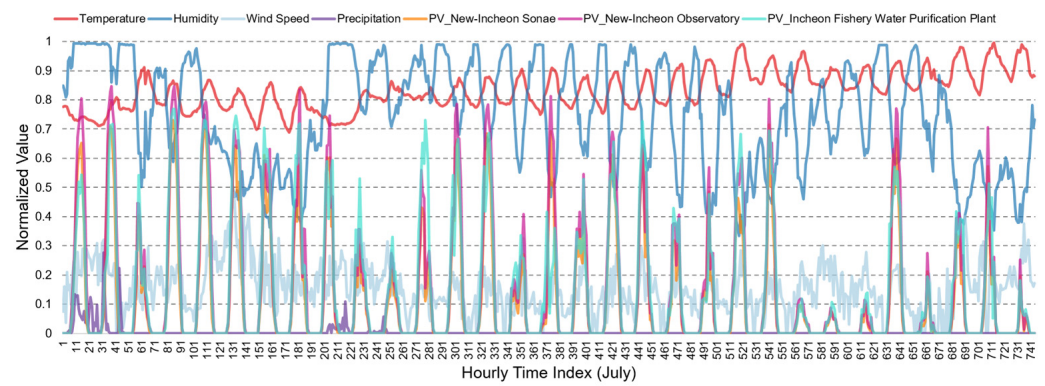


Figure 1. Min–max normalized meteorological and solar photovoltaic (PV) power data in Incheon for July 2019. The hourly time index runs from 1 a.m. on the 1st to midnight on the 31st.

2.2. Model Construction

Figure 2 shows the overall architecture of the proposed solar PV power generation forecasting method. First, we divided the preprocessed dataset into a training set (2018) and a test set (2019) in a 5:5 ratio as described earlier. We performed two stages of optimization techniques on nine DNN models and derived final predictions. The details of this study are described in the following subsections.

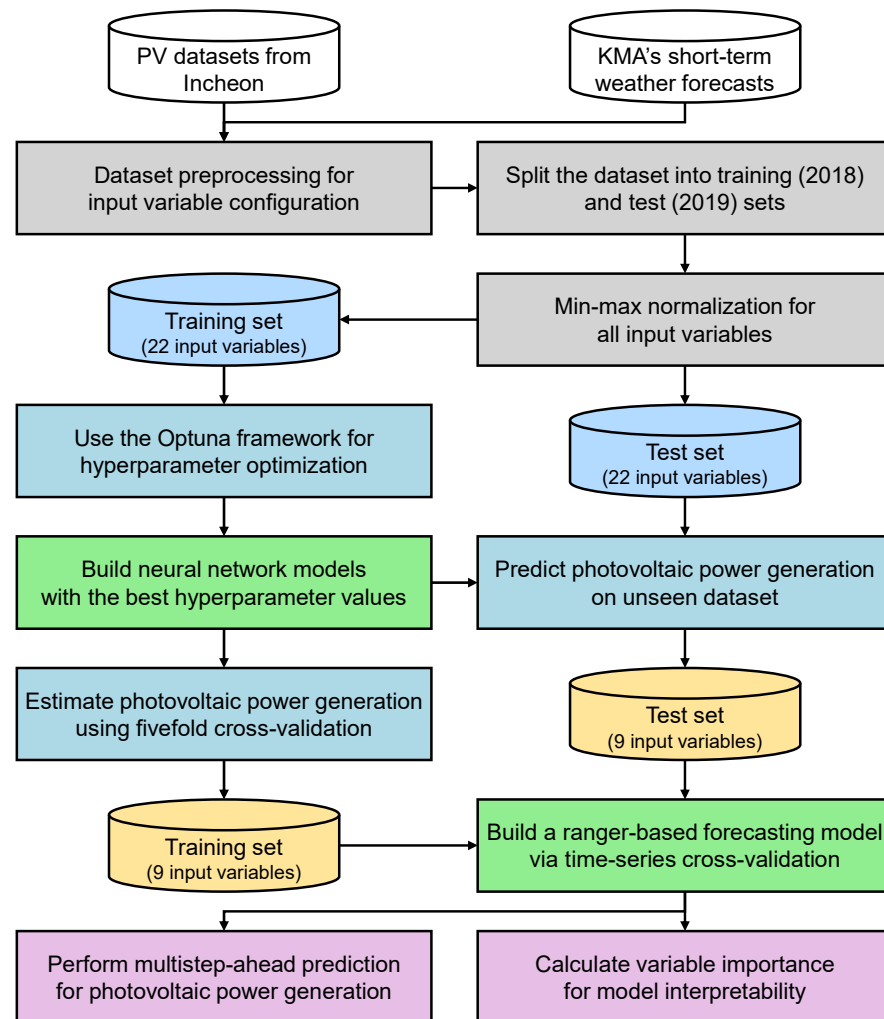


Figure 2. Procedure for multistep-ahead solar PV power generation forecasting.

2.2.1. Stage 1: Optimized Deep Neural Network Architecture with Optuna

A multilayer perceptron (MLP), also known as a typical NN configuration, allows computers to learn tasks by example, as shown in Figure 3 [46]. It is similar to a schematic that guides the computer in formulating a solution to a problem. The framework of an MLP consists of individual elements, called perceptrons, organized in layers. An MLP conventionally includes three types of layers: the input layer, which captures data that the computer uses to make a prediction; one or more hidden layers, which relevant pertinent information from the input layer to refine the prediction; and the output layer, which provides the final result based on the synthesized information from the hidden layers [46,47]. We used Equation (6), which integrates the input data, neural connections (weights), and an activation function, to compute the output values of the neurons in the hidden layer of an MLP.

$$y_j = \varphi(\sum w_{ij} \times x_i + b_i) \quad (6)$$

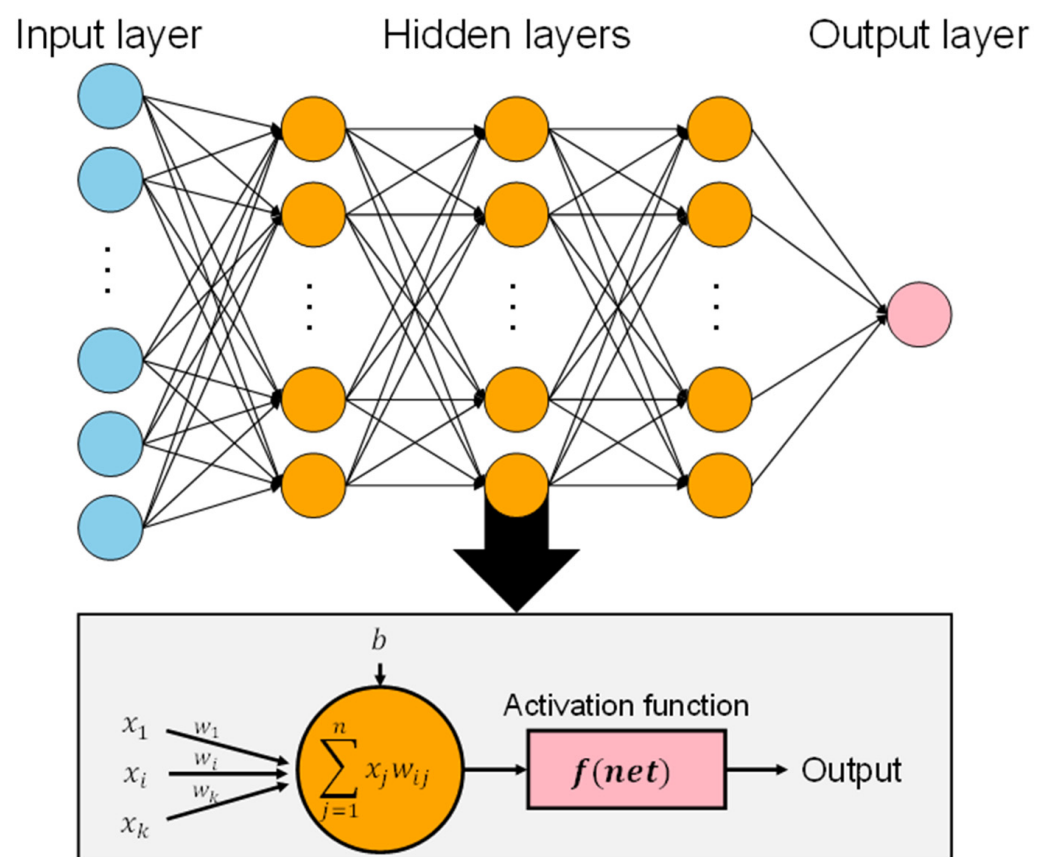


Figure 3. Multilayer perceptron architecture.

The input layer of an MLP consists of neurons, each of which is represented by x_i . Synaptic weights, abbreviated as w_{ij} , reflect the connections between neurons in the input and hidden layers. The activation function (φ) controls the output of the hidden layer neurons. When an MLP contains more than two hidden layers, it is referred to as a DNN, indicating a deeper level of computational complexity [47,48]. Biases (b_i) are added to the inputs of the activation function to help the network make more accurate predictions. Weights serve as important links not only between the input and hidden layers, but also between multiple hidden layers and between the last hidden layer and the output layer, and they play an important role in information processing and modeling. A feature of MLPs is their ability to process information in a distributed manner, with each neuron acting independently. This makes the system fault-tolerant because it can continue to learn and process data even if some neurons fail [48].

MLPRegressor is one of the components of scikit-learn, the widely used ML package in Python. It is a DL model for regression tasks that is adept at predicting numerical outputs from given input features [49]. While DNN models are typically constructed using frameworks such as TensorFlow, Keras, or PyTorch, which excel in GPU environments, MLPRegressor provides an effective benchmark for utilities and government organizations managing solar PV systems, particularly in scenarios where investment in advanced computing infrastructure is not feasible. MLPRegressor facilitates efficient model deployment on lower-capacity systems, underscoring its role as a practical solution in resource-constrained environments.

In addition, MLPRegressor can produce excellent results on structured datasets [29,48]. Its performance can be significantly improved by tuning key hyperparameters: hidden layer sizes, activation functions, batch size, learning rate, and maximum iterations. Therefore, to address the challenge of solar PV power generation prediction on low-power systems, we decided to use scikit-learn's MLPRegressor and adjust these hyperparameters for optimal results. This approach balances the need for cost efficiency and effective use of computational resources, ensuring that our model is widely applicable and can operate effectively in constrained computing environments, making it an excellent benchmark model.

The configuration of the hidden layer has a significant impact on the efficiency of the network, highlighting the importance of considering the number of layers and nodes, as well as the activation function, when designing the network [28]. Although increasing the number of hidden layers often improves network efficiency, it also increases the possibility of overfitting [28,29]. Identifying the optimal number of hidden layers to prevent overfitting can be particularly challenging, especially for those not specialized in ML and DL, such as energy experts. This complexity arises because the development of DL models can yield different results based on different training conditions, and is particularly resource-intensive [29]. To mitigate these challenges, we first built several DNN models with different hidden layer structures. For our prediction efforts, we created nine DNN models with the number of layers ranging from 4 to 12 within the training set.

Traditional hyperparameter tuning techniques have been extended to include gradient-based optimization, evolutionary algorithms, simulated annealing, particle swarm optimization, hyperband, gradient-based optimization, random search, and Bayesian optimization to improve DL models [50,51]. While these methods expand the range of tools available to improve model performance, they often share the same drawbacks: high computational requirements, significant time commitment, and a complexity that can be intimidating to practitioners not trained in ML, such as those working in the energy industry. Under severe time and computational resource constraints, these approaches may not provide the best model efficiency and scalability due to their thorough and often random search through hyperparameter spaces.

Optuna [48,52], a versatile Python toolkit, provides a unified interface for refining hyperparameters in ML constructs to increase their effectiveness. Hyperparameters are the pre-training configurations of algorithms, as opposed to the parameters that are adjusted during the training process itself. Within the architecture of an NN, critical hyperparameters include the number of hidden layers, the learning rate, and the intensity of regularization. Designed to streamline the hyperparameter optimization process, Optuna extends an intuitive and customizable application programming interface for architecting ML models and defining the scope of hyperparameter exploration. This suite uses a variety of methods to traverse the hyperparameter terrain, including the Tree-structured Parzen Estimator, as well as random and grid searches, to find the best hyperparameters that improve metrics such as accuracy or F1 score.

Optuna is unique in its ability to synchronize simultaneous trials, which are different evaluations of a model configured with different hyperparameter combinations. This feature drives Optuna's ability to traverse the hyperparameter landscape with increased speed and precision. A key feature of Optuna is its early termination mechanism, which allows the optimization effort to be halted when the likelihood of further trials refining

the results is minimal, thereby optimizing resource utilization and mitigating the risk of overfitting. In addition, Optuna includes a tracking API that provides insight into the trajectory of the optimization and detailed records of each trial, essential for the analysis and refinement of the optimization strategy. We defined the hyperparameter search space as shown in Table 4 and set the number of iterations in Optuna to 1000. We then used Optuna through fivefold cross-validation on the training set to determine the optimal hyperparameter values for each DNN model, as shown in Figure 4.

Table 4. List of hyperparameters for optimal deep neural network (DNN) model construction.

Hyperparameter	Definition	Range
<i>hidden_layer_sizes</i>	Number of neurons in each hidden layer, for 2 to 10 layers	2–10 hidden layers, each with 1–40 (Step: 1) [48]
<i>activation</i>	Activation function for the hidden layer	<i>relu</i> [29]
<i>solver</i>	The solver for weight optimization	<i>adam</i> [29]
<i>alpha</i>	L2 penalty (regularization term) parameter	0.0001–0.001 (Step: 0.0001) [48]
<i>batch_size</i>	Size of minibatches for stochastic optimizer	5–100 (Step: 1) [48]
<i>learning_rate</i>	Learning rate schedule for weight updates	<i>constant, adaptive</i> [48]
<i>learning_rate_init</i>	Initial learning rate	0.0001–0.1 (Step: 0.0001) [48]
<i>max_iter</i>	Maximum number of iterations	100–2000 (Step: 10) [48]

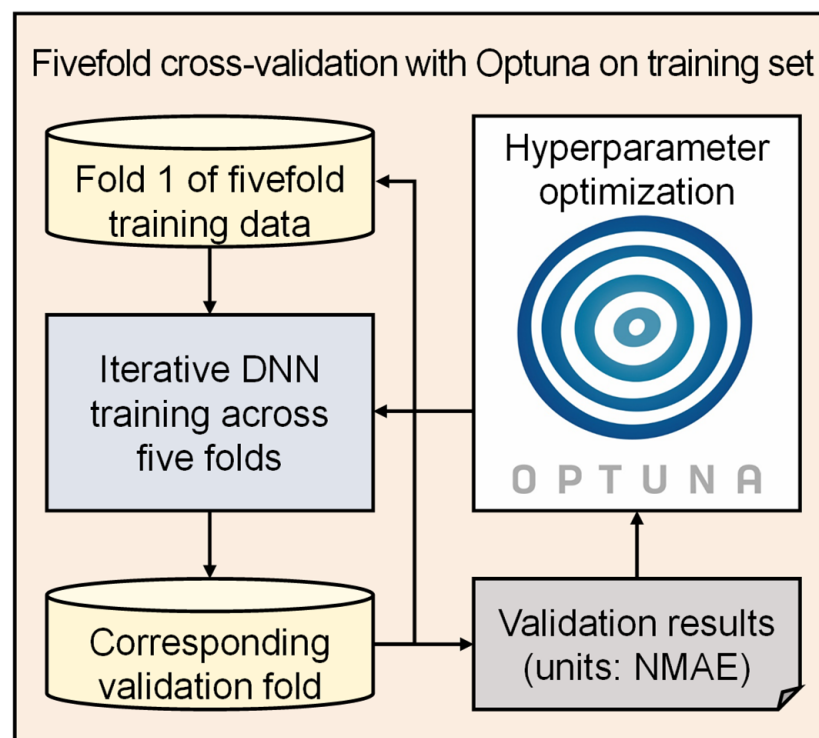


Figure 4. Optimization of a deep neural network (DNN) model with fivefold cross-validation using Optuna. NMAE represents negative mean absolute error.

In this paper, we constructed nine DNN models with 2 to 10 hidden layers in the training set and carefully determined the optimal hyperparameter settings for each model using Optuna’s fivefold cross-validation. This preliminary step ensured that we identified the most effective configurations to improve the predictive accuracy of our models.

In addition, we took a strategic approach to the challenge of constructing a sufficient validation set within a limited timeframe, especially when a separate validation set may not have been feasible due to the constraints of not having an extended training period. We performed another round of fivefold cross-validation on the training set based on these

optimized hyperparameters to prepare adequate training data for our meta-learning model within the stacking ensemble framework. This method allowed us to ensure robust learning from even a one-year training dataset, effectively overcoming potential limitations in the availability of validation datasets. In parallel, we used the entire training dataset, now fully trained with the optimized hyperparameters, to make preliminary solar PV power generation predictions on the test set. This comprehensive approach was able to maximize the predictive capabilities of our models under the specific constraints of the study.

2.2.2. Stage 2: Ranger-Based Online Learning Model for Multistep-Ahead Prediction

Even with DNN models optimized by Optuna, the high computational load of DNNs for online learning poses a challenge, especially for real-time energy management. To address this issue, our stacking ensemble method, which integrates different DNNs with an RF meta-regression model, leverages the predictive capabilities of DNNs while mitigating their computational demands. This approach provides significant benefits to energy managers by enabling efficient, real-time prediction of solar PV power generation, which is critical for optimizing energy distribution and demand forecasting. By combining the analytical depth of DNNs with the operational efficiency of RF, the proposed method can provide a practical solution for advancing energy management practices, highlighting the originality and applicability of our approach in the energy sector.

RF [53,54] is a prime example of a bagging ensemble technique. It constructs multiple decision trees (DTs) trained on randomly selected subsets of variables (features) and outputs the result by averaging (for regression tasks) or majority voting (for classification tasks) over the predictions of all DTs [54]. Efficient for online learning and requiring minimal hyperparameter tuning, RF works efficiently on large datasets and shows excellent performance in areas such as bioinformatics and time series prediction because it can handle large numbers of input variables without the need for variable elimination [55,56]. Its robust performance and ability to handle multicollinearity make it suitable for handling highly correlated inputs from DNN models. In addition, RF generally requires less hyperparameter tuning than other ML methods and often provides satisfactory performance even with default hyperparameter settings [57]. We focus on two commonly adjusted RF hyperparameters for model training: the number of trees to grow (*n_estimators* for Python and *nTree* for R) and the number of variables considered for partitioning at each tree node (*max_features* for Python and *mTry* for R) [56,57].

We selected the RF algorithm based on its adaptability to the specific needs and constraints of this study, rather than on claims of universal superiority [58,59]. The implementation of online learning, which selects optimal hyperparameters at each time point for model training and prediction, poses significant challenges in real-world industrial settings due to its computational and time requirements [33]. RF's adaptability and ease of tuning are particularly valuable in these settings. RF is characterized by robust performance with minimal need for hyperparameter optimization, in contrast to DL models that often require careful tuning of hyperparameters to achieve peak performance. Furthermore, its effectiveness as a meta-regression model in a stacking ensemble highlights its versatility. In addition, RF correctly handles multicollinearity, ensuring model robustness for highly correlated input variables [60]. This feature allows for more effective learning and final prediction of solar PV power generation estimation and prediction values in the training and test sets derived from DNN models. Therefore, the adoption of RF was based on its balanced learning capabilities and conformity with the requirements and limitations of the study [61,62].

The *RandomForestRegressor* implementation in Python and the *randomForest* package in R are widely appreciated for their rich functionality. However, they are not ideally optimized for high-dimensional datasets. Furthermore, a major drawback is the slow execution speed of the model. The Ranger, an innovative software package, has been developed to overcome these limitations and increase efficiency for high-dimensional data analysis [63]. Efficient memory management is achieved by minimizing data duplication,

storing node information in compact data structures, and freeing memory in a timely manner. The Ranger package introduces two innovative partitioning methods. The first method sorts feature values by index before partitioning, while the second method splits raw values directly and organizes them afterward. These methods optimize the runtime for the main and minor nodes used in the first and second scenarios, respectively. These runtime optimization methods make Ranger a powerful tool for RF implementations in complex scenarios.

The essence of stacking ensemble learning is to orchestrate a diverse collection of models, such as DNNs, to work in parallel and synergize their predictions through a meta-regression framework, such as RF, to refine the overall prediction accuracy [29,64]. However, because many of these weak learners are based on ML or DL methods that rely heavily on data characteristics, stacking ensemble learning may have limitations in improving solar PV power generation predictions. As a result, ML or DL methods may struggle to achieve high accuracy on out-of-sample (unseen) datasets that differ significantly from the in-sample (training) data. For example, if the observed PV power in the test dataset significantly exceeds that in the training dataset, a model calibrated to the latter may not effectively predict escalation [61]. In addition, achieving satisfactory predictive performance with insufficient data becomes difficult, especially when the available training data are scarce [61,65].

We used R Ranger to construct an online learning model that uses time series cross-validation (TSCV) to address these challenges [65]. TSCV emphasizes the evaluation of multiple prediction horizons within each training set. Additional training sets were used according to the planned time period, each containing one observation not included in the previous training set. We designed the test set to range from one hour to one day (up to 11 h) after the current period to allow for multistep-ahead prediction of solar PV power generation, as shown in Figure 5. The prediction accuracy was calculated at each time point and the results were averaged to evaluate the effectiveness of the prediction model. To train the Ranger model, nine input variables were selected, encapsulating predictions from DNNs with 2 to 10 hidden layers. In addition, in accordance with best practices and to tailor our model specifically for regression tasks, we set the number of trees to 128 and the number of features to 3, reflecting one-third of our nine input variables for optimized regression [57,66].

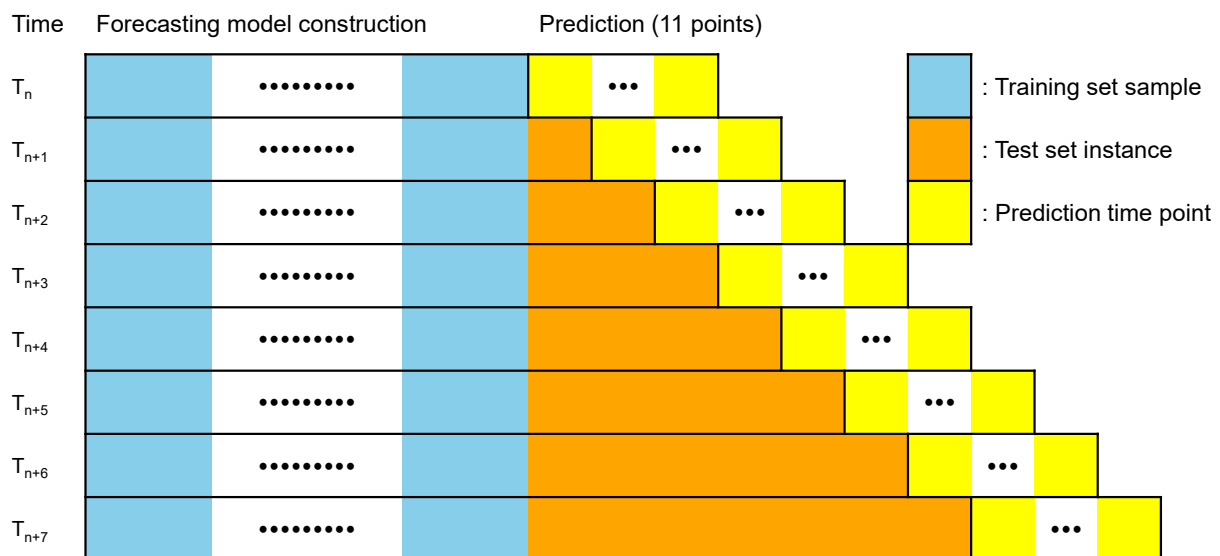


Figure 5. Time series cross-validation for multistep-ahead solar PV power generation forecasting.

The proposed method excels in predicting solar PV power output by combining ensemble learning with TSCV. This approach could overcome the limitations of static DL

algorithms such as DNN, LSTM, Bi-LSTM, GRU, and one-dimensional CNN (1D-CNN) by progressively incorporating fresh data to gradually increase the prediction accuracy. The proposed method captures complicated nonlinear interactions in the data by using a two-stage NN optimization that incorporates different DNNs in the first stage and an RF algorithm as a meta-regression model in the second stage. It also uses incremental learning to adapt to new trends and patterns as more data becomes available. Most importantly, this approach is optimized for central processing unit (CPU) usage, ensuring broad application in real-world environments with limited computing resources. As a result, even with a small initial dataset, the proposed method ensures robust learning and accurate prediction, which is important for ML applications that collect data over time.

3. Results

3.1. Experimental Setup

In this research, we established an experimental framework to test our proposed approach for solar PV power generation forecasting 11 steps (one day) in Incheon, South Korea. The experimental hardware consisted of an Intel(R) Core(TM) i7-9700 CPU @3.00 GHz and 64 GB RAM. Software tools included Anaconda 22.9.0 and Python 3.8.0 for data pre-processing, and RStudio version R-4.2.2 along with R version 4.2.2 (2022-10-31 UCRT) for additional data processing and development of the Ranger-based online learning model. This setup was critical for evaluating and improving the accuracy of the solar PV power generation prediction model. We set the random state and the random seed to 42 and 1234 in Python and R, respectively, to ensure the reproducibility of the experiment and to allow direct comparison of models trained under identical conditions.

Two statistical measures were used to evaluate the accuracy of the prediction models: MAE, which is calculated as the average of the absolute differences between the predicted and actual values, and RMSE, which measures the square root of the average squared differences between the predicted and actual values, defined by the following Equations (7) and (8), respectively:

$$MAE = \sum |P_t - A_t| / n, \quad (7)$$

$$RMSE = \sqrt{(\sum (P_t - A_t)^2) / n}, \quad (8)$$

where A_t and P_t denote the actual and predicted values at time t , n is the number of observations.

3.2. Experimental Results

In this study, we meticulously conducted experiments using the New-Incheon Sonae, New-Incheon Observatory, and Incheon Fishery Water Purification Plant test sets (2019) from Incheon, South Korea as unseen data to evaluate the performance of our proposed model. Our main objective was to compare our proposed model with a set of benchmark models, which had previously demonstrated remarkable performance in predicting solar PV power generation. First, we constructed an RF model using Ranger as a benchmark model for multistep-ahead forecasting, using TSCV with 22 input variables. Then, we constructed DL models for multistep-ahead forecasting, starting with robust time series forecasting models from the RNN family, including LSTM, Bi-LSTM, and GRU models [23]. In addition, we developed seven state-of-the-art models that incorporate attention mechanisms (Att) [67–73]. These steps allowed us to comprehensively compare the established benchmark models, known for their effectiveness in various domains, with our proposed model. To create a comparable environment for multistep-ahead solar PV power generation forecasting, we configured the time steps from 1 to 11 using a many-to-many approach. We adhered to the core architectural frameworks of the models as described in the research articles, and fine-tuned the hyperparameters using Optuna to ensure optimal performance.

The benchmark models include:

- Att-LSTM: Zhou et al. [67] developed the Att-LSTM model using a hybrid ensemble DL framework with two LSTM NNs focused on temperature and power output for short-

term PV power generation. The incorporation of an attention mechanism improved the prediction accuracy by prioritizing significant input features.

- Att-Bi-LSTM: He et al. [68] constructed the Att-Bi-LSTM model, which combines a Bi-LSTM architecture and attention mechanisms for predicting PV power generation from solar PV systems, and demonstrated superior accuracy by selecting environmental factors using the Pearson coefficient.
- Att-GRU: Jung et al. [69] introduced the Att-GRU-based energy forecasting model, an attention-based GRU approach for multistep-ahead electrical load forecasting, which outperforms other models by emphasizing crucial variables in response to sudden changes in power consumption.
- Att-1D-CNN: Wu et al. [70] proposed the Att-1D-CNN model, which uses a CNN and informer approach, and achieves accurate solar PV power generation prediction by analyzing data correlations, significantly improving the prediction accuracy over traditional models.
- Att-TCN: Ren et al. [71] introduced the Att-TCN model, a novel dual-channel TCN that combines a multi-head attention mechanism with TCN to extract spatiotemporal features, and demonstrated superior prediction performance for solar PV power generation forecasting.
- Att-GRU-TCN: Xiao et al. [72] proposed the Att-GRU-TCN model for probabilistic power flow in multi-microgrids, which integrates GRU and TCN with an attention mechanism to improve reliability and efficiency in networks with incomplete information.
- Att-Bi-GRU-TCN: Zhou et al. [73] developed the Att-Bi-GRU-TCN model for short-term solar PV power generation forecasting, which uses a two-step approach with TCN and Bi-GRU to capture both short-term and long-term dependencies, ensuring robust forecasting accuracy.

In Tables 5–10, we observed the exceptional performance of the proposed method. This model showed excellent predictive capabilities with the smallest MAE and RMSE values among the multistep-ahead predictions. For example, the proposed method showed an average MAE of 149.53 kW and RMSE of 202.00 kW for the New-Incheon Sonae dataset, which is significantly lower than the average MAE of up to 171.11 kW and RMSE of up to 233.66 kW of the benchmark models in Table 5. The model's effective implementation of online learning and a sophisticated stacking ensemble approach can achieve a high level of accuracy in predicting solar PV power generation for the New-Incheon Sonae, New-Incheon Observatory, and Incheon Fishery Water Purification Plant datasets. The stacking ensemble technique could effectively combine the predictive strengths of different DNN models, resulting in a consistent and fine-tuned prediction.

Notably, both our model and the Ranger model, which incorporates online learning, routinely outperform typical DL models. The results may demonstrate the effectiveness of online learning in adapting to new, real-time data, which is an important feature for models operating in dynamic situations. However, it is critical to understand the constraints experienced. The DL models struggled to adapt to a training set spanning one year, indicating a weakness in their ability to learn from large amounts of temporal data in a short period of time. In addition, the lack of solar irradiance as an input variable limits the ability to improve prediction accuracy. Since solar irradiance is such an important aspect of PV power generation, its inclusion in future models could lead to significant improvements in prediction accuracy.

To evaluate our proposed model for single-day-ahead forecasting in Incheon, we compared it with several benchmark models. For a thorough evaluation, we analyzed the performance over different time periods, including quarterly and overall metrics. We evaluated the 11-step-ahead (day-ahead) forecast values of the proposed method by measuring the forecast accuracy. First, we adopted a statistical method from the persistence model, which relies on data from the corresponding time of the previous day. For example, to forecast solar PV power generation at 14:00 on June 8, we used data from 14:00 on June 7. We also used the hold-out technique to construct the Ranger-based RF model with

22 input variables. In addition, we evaluated the prediction values of nine DNN models configured for one-step prediction, whose performance was enhanced by hyperparameter optimization using Optuna.

In the extended analysis, we found a striking trend: over time, our model with online learning widens the performance gap in prediction accuracy over other models, as shown in Tables 11–13. In particular, the proposed method showed a consistent improvement in accuracy for day-ahead solar PV power generation forecasting, with a significant reduction in MAE and RMSE values. In the New-Incheon Sonae dataset, this model maintained a lower average MAE and RMSE of 151.66 kW and 204.72 kW, respectively, compared to other DNN models with higher layers, which showed MAEs and RMSEs increasing to 185.54 kW and 255.43 kW, respectively. This pattern indicates that the proposed method's online learning capability is not only effective in adapting to immediate data trends but also improves its prediction accuracy over time, outperforming benchmark models. We concluded that the model's ability to continuously learn and integrate new information plays a critical role in its sustained superior performance.

Tables 14–16 present the results of a comprehensive evaluation of the day-ahead forecasting models, showing their varying effectiveness under different weather conditions. Notably, the proposed method consistently outperformed not only the benchmark Persistence model but also other models, such as Ranger and various DNN configurations, in terms of accuracy under clear weather conditions by demonstrating lower MAE and RMSE. Specifically, for the New-Incheon Sonae dataset, the proposed method achieved an MAE of 141.17 kW and an RMSE of 189.96 kW, surpassing the Persistence model's MAE and RMSE of 148.04 kW and 226.16 kW, respectively, as well as those of the Ranger and DNN models.

Conversely, the performance of the proposed method under rainfall conditions dropped below that of the Persistence model, which proved to be more accurate, as reflected in the MAE and RMSE metrics. For example, for the Incheon Fishery Water Purification Plant dataset during rain events, our model recorded an MAE of 162.19 kW, while the Persistence model showed a lower MAE of 132.16 kW. This discrepancy highlights the current limitation of our dataset, which spans two years, with one year allocated to the training set. The limited representation of rainy conditions in the dataset likely led to the observed performance gap, although our model still outperformed the Ranger and DNN models even under these conditions.

In Figure 6, we revisit the timeline first introduced in Figure 1, contrasting projected and actual solar PV power generation data for July 2019. While the model effectively reflects general trends in energy production, it occasionally shows shortcomings in identifying sudden declines in power generation.

The reasons for these discrepancies vary. Despite its robust design, the model's internal workings may not fully capture the nuanced complexities of PV operations. In addition, the potential scarcity of solar irradiance metrics could undermine the accuracy of the forecast. Furthermore, location differences between our data points and Incheon's meteorological readings may have resulted in less accurate representations of local weather patterns, which are influenced by subtle microclimatic variations.

To address these findings, subsequent research efforts will integrate finer-grained weather data and refine the model's mechanisms to more accurately reflect the dynamic nature of PV production. The expected improvements from incorporating advanced DL strategies aim to significantly refine the predictive accuracy of the proposed method. The expected improvements go beyond creating a reliable tool for forecasting PV generation; they will improve grid management and energy distribution strategies amidst the variability inherent in renewable energy sources.

Table 5. Mean absolute error (MAE) comparison across multistep-ahead prediction models for the New-Incheon Sonae dataset (unit: kW).

Step	Ranger	LSTM [24]	Bi-LSTM [24]	GRU [24]	Att-LSTM [67]	Att-Bi-LSTM [68]	Att-GRU [69]	Att-1D-CNN [70]	Att-TCN [71]	Att-GRU-TCN [72]	Att-Bi-GRU-TCN [73]	Ours
1	152.15	170.97	173.56	171.32	172.29	165.32	163.85	169.03	165.04	170.55	166.99	142.87
2	153.82	165.58	173.97	161.89	172.05	165.79	165.37	172.68	165.80	172.81	168.75	146.58
3	155.07	166.01	172.23	163.85	172.46	165.51	168.67	169.40	172.06	172.30	170.14	148.71
4	155.32	166.27	173.12	166.56	171.47	165.63	168.48	166.29	174.60	172.12	170.61	149.52
5	155.62	167.39	172.25	165.86	172.97	165.00	167.51	167.12	176.10	171.37	172.09	150.47
6	156.08	171.34	171.81	164.26	173.20	167.55	170.65	168.62	176.29	171.83	171.10	150.64
7	156.52	177.69	169.89	164.92	173.21	166.89	167.48	170.93	176.95	173.85	172.34	150.94
8	156.13	173.54	168.21	165.60	171.94	169.11	165.94	171.11	177.94	172.23	171.12	151.07
9	156.29	170.43	168.32	165.00	170.34	168.09	165.17	171.35	176.90	172.98	169.81	151.23
10	156.39	173.03	168.66	162.81	165.75	165.13	165.03	169.80	177.73	171.85	167.15	151.11
11	156.55	180.00	163.19	160.60	163.45	162.26	169.09	169.98	176.16	168.63	164.99	151.66
Avg.	155.45	171.11	170.47	164.79	170.83	166.02	167.02	169.66	174.14	171.87	169.55	149.53

Table 6. Root mean squared error (RMSE) comparison across multistep-ahead prediction models for the New-Incheon Sonae dataset (unit: kW).

Step	Ranger	LSTM [24]	Bi-LSTM [24]	GRU [24]	Att-LSTM [67]	Att-Bi-LSTM [68]	Att-GRU [69]	Att-1D-CNN [70]	Att-TCN [71]	Att-GRU-TCN [72]	Att-Bi-GRU-TCN [73]	Ours
1	204.24	226.73	236.26	225.94	235.27	226.33	222.45	229.64	229.44	236.28	229.76	192.52
2	206.53	222.35	237.06	219.66	236.22	227.36	226.45	234.44	230.51	239.73	232.96	197.94
3	208.05	226.82	234.84	224.09	236.41	225.69	229.53	230.40	237.60	238.70	235.03	201.16
4	208.42	227.68	235.80	226.63	235.78	226.84	229.76	224.21	240.84	237.19	235.25	202.04
5	208.87	226.87	235.60	226.79	236.94	226.69	227.79	225.44	242.42	236.46	235.55	203.30
6	209.61	227.04	235.00	226.46	237.15	230.58	228.38	229.34	242.05	236.57	234.64	203.63
7	209.96	229.70	232.59	227.50	237.34	229.70	224.41	233.84	242.56	238.90	236.76	203.81
8	209.54	228.46	231.02	228.68	235.15	232.15	223.28	234.60	244.05	237.32	235.10	204.25
9	209.86	226.48	231.05	227.13	233.73	228.75	222.50	233.76	243.54	239.02	234.28	204.29
10	210.00	232.52	230.14	222.13	226.25	225.56	219.84	230.65	244.64	236.89	231.69	204.36
11	210.20	247.36	222.70	215.02	219.97	223.93	220.78	231.85	242.25	232.58	228.75	204.72
Avg.	208.66	229.28	232.91	224.55	233.66	227.60	225.01	230.74	239.99	237.24	233.62	202.00

Table 7. MAE comparison across multistep-ahead prediction models for the New-Incheon Observatory dataset (unit: kW).

Step	Ranger	LSTM [24]	Bi-LSTM [24]	GRU [24]	Att-LSTM [67]	Att-Bi-LSTM [68]	Att-GRU [69]	Att-1D-CNN [70]	Att-TCN [71]	Att-GRU-TCN [72]	Att-Bi-GRU-TCN [73]	Ours
1	126.63	146.56	141.96	191.38	144.77	145.45	145.98	154.40	138.39	143.33	144.29	118.73
2	128.40	139.88	143.10	174.92	145.17	147.26	150.80	153.41	136.64	143.37	144.92	122.98
3	129.40	142.76	143.14	163.30	144.14	145.85	149.78	155.18	137.78	143.48	144.53	124.59
4	130.06	143.70	143.28	158.55	142.43	145.92	153.24	156.50	137.56	143.40	146.69	125.74
5	130.41	142.99	143.27	157.53	141.06	147.70	150.45	156.86	139.61	142.66	146.39	126.16
6	130.78	144.08	143.16	155.06	141.35	146.56	145.64	164.68	139.75	142.57	146.01	126.71
7	130.78	144.76	143.37	148.62	141.14	146.58	145.38	164.83	140.24	142.23	143.79	126.57
8	130.98	143.90	142.63	148.32	142.35	146.77	144.11	159.99	140.56	144.31	142.67	126.76
9	130.77	140.44	141.23	147.79	142.55	144.57	143.02	153.87	142.03	144.39	141.90	126.70
10	130.72	136.36	140.78	144.18	140.10	141.78	142.18	148.90	142.76	144.07	139.21	126.94
11	130.83	133.12	138.21	143.37	135.78	139.20	139.44	160.12	142.43	143.87	137.90	127.20
Avg.	129.98	141.69	142.19	157.55	141.89	145.24	146.37	157.16	139.80	143.42	143.48	125.37

Table 8. RMSE comparison across multistep-ahead prediction models for the New-Incheon Observatory dataset (unit: kW).

Step	Ranger	LSTM [24]	Bi-LSTM [24]	GRU [24]	Att-LSTM [67]	Att-Bi-LSTM [68]	Att-GRU [69]	Att-1D-CNN [70]	Att-TCN [71]	Att-GRU-TCN [72]	Att-Bi-GRU-TCN [73]	Ours
1	176.54	203.94	205.31	245.31	211.65	206.83	212.93	205.23	200.80	206.97	207.98	156.64
2	179.27	200.98	206.21	230.58	212.86	212.44	217.08	204.29	200.31	207.53	210.68	163.03
3	180.54	204.45	207.56	218.74	212.09	210.36	217.09	205.52	202.18	209.09	209.92	165.41
4	181.43	203.38	208.95	213.52	210.11	211.39	221.39	209.32	203.46	208.93	212.78	167.02
5	182.25	202.38	208.92	212.33	207.99	212.53	217.06	209.54	205.70	207.77	212.90	167.85
6	182.65	203.52	207.80	210.77	208.18	211.96	210.09	210.93	205.67	207.13	211.67	168.52
7	182.70	204.84	209.12	206.93	206.92	211.91	207.51	211.28	205.53	206.75	208.79	168.56
8	183.04	203.45	208.31	205.01	206.79	211.18	206.23	206.25	206.05	207.54	206.55	168.69
9	182.73	198.70	208.02	204.08	207.10	207.22	203.16	201.53	207.19	208.87	204.72	168.81
10	182.57	191.73	207.01	203.73	202.21	202.93	203.39	200.14	208.61	208.39	199.84	168.74
11	183.00	189.31	202.51	203.75	195.36	198.34	196.87	211.18	207.70	208.15	196.32	169.24
Avg.	181.52	200.61	207.25	214.07	207.39	208.83	210.25	206.84	204.84	207.92	207.47	166.59

Table 9. MAE comparison across multistep-ahead prediction models for the Incheon Fishery Water Purification Plant dataset (unit: kW).

Step	Ranger	LSTM [24]	Bi-LSTM [24]	GRU [24]	Att-LSTM [67]	Att-Bi-LSTM [68]	Att-GRU [69]	Att-1D-CNN [70]	Att-TCN [71]	Att-GRU-TCN [72]	Att-Bi-GRU-TCN [73]	Ours
1	140.26	147.83	143.76	179.15	156.70	165.53	152.46	151.25	152.65	159.05	155.23	134.30
2	142.06	148.27	145.05	163.19	158.16	163.33	154.90	150.67	153.34	161.40	156.06	139.08
3	142.98	147.53	147.99	159.11	158.94	167.27	155.12	154.25	156.64	160.22	156.29	140.63
4	143.27	146.01	148.47	159.82	158.15	166.84	156.73	155.43	158.63	161.80	157.30	141.80
5	143.68	147.00	147.38	154.41	157.28	167.10	153.75	156.82	164.01	162.62	156.75	142.77
6	144.22	149.24	146.16	153.63	157.16	167.89	153.60	155.36	164.52	164.39	157.73	143.18
7	144.25	151.27	145.19	166.88	157.57	167.25	152.89	155.40	165.77	168.45	158.31	143.65
8	144.44	154.03	143.37	172.64	158.12	163.71	152.79	155.79	166.31	168.32	158.46	143.31
9	144.50	153.78	143.74	167.57	157.95	160.42	150.29	154.76	167.54	172.15	159.16	143.64
10	144.45	153.34	144.01	161.81	152.69	154.48	146.53	153.74	167.42	171.12	157.51	143.58
11	144.47	152.60	145.95	163.11	148.41	157.31	149.34	151.17	168.10	168.09	156.13	144.76
Avg.	143.51	150.08	145.55	163.76	156.47	163.74	152.58	154.06	162.27	165.24	157.18	141.88

Table 10. RMSE comparison across multistep-ahead prediction models for the Incheon Fishery Water Purification Plant dataset (unit: kW).

Step	Ranger	LSTM [24]	Bi-LSTM [24]	GRU [24]	Att-LSTM [67]	Att-Bi-LSTM [68]	Att-GRU [69]	Att-1D-CNN [70]	Att-TCN [71]	Att-GRU-TCN [72]	Att-Bi-GRU-TCN [73]	Ours
1	191.17	199.32	198.02	223.15	222.31	227.75	213.35	209.16	218.36	225.33	221.23	180.06
2	193.58	202.74	204.28	209.48	224.15	226.52	218.43	209.35	218.42	229.17	221.65	186.61
3	194.71	201.54	205.54	203.77	225.12	230.32	220.53	215.95	222.55	228.46	222.53	189.35
4	195.33	200.84	205.01	202.72	223.25	230.15	223.18	217.49	225.26	230.92	223.74	191.21
5	196.04	204.18	203.33	199.51	222.76	233.76	219.63	218.88	232.78	232.25	221.73	192.33
6	196.69	207.98	202.03	204.37	223.28	234.27	219.32	218.51	232.86	233.87	223.38	193.02
7	196.64	209.91	202.12	220.68	223.32	231.16	218.15	219.19	234.09	239.09	223.95	193.81
8	196.95	211.28	200.49	228.41	222.49	227.35	217.97	220.03	234.38	238.62	224.20	193.29
9	197.08	209.77	201.02	221.48	222.12	222.39	212.89	219.16	236.33	243.50	224.28	193.41
10	196.97	206.69	200.95	213.13	215.67	214.71	207.69	218.26	236.41	241.91	221.63	193.87
11	196.84	205.10	201.74	214.04	206.18	222.28	201.86	211.45	237.45	237.20	219.51	194.71
Avg.	195.64	205.40	202.23	212.80	220.97	227.33	215.73	216.13	229.90	234.57	222.53	191.06

Table 11. MAE and RMSE comparisons across day-ahead prediction models for the New-Incheon Sonae dataset (unit: kW). HL indicates the number of hidden layers.

Model	Jan.–Mar.		Apr.–Jun.		Jul.–Sep.		Oct.–Dec.		Avg.	
	MAE	RMSE	MAE	RMSE	MAE	RMSE	MAE	RMSE	MAE	RMSE
Persistence	155.98	228.90	145.03	223.95	152.23	217.00	137.54	231.26	147.66	225.33
Ranger	146.67	203.00	163.98	226.73	172.26	227.08	178.09	244.83	165.35	226.02
DNN (HL: 2)	153.22	216.03	172.61	241.38	181.96	239.90	179.98	251.56	172.05	237.68
DNN (HL: 3)	152.82	214.98	167.46	234.08	170.42	224.52	175.35	245.54	166.58	230.13
DNN (HL: 4)	149.26	210.65	169.05	237.00	179.26	237.94	176.94	247.87	168.73	233.88
DNN (HL: 5)	151.42	212.71	171.57	239.27	184.31	242.80	178.59	250.63	171.58	236.90
DNN (HL: 6)	156.61	219.92	174.89	241.31	175.93	232.83	177.55	247.88	171.32	235.79
DNN (HL: 7)	149.89	212.75	168.68	236.05	179.25	235.15	174.57	246.72	168.19	233.09
DNN (HL: 8)	160.53	230.99	193.44	262.10	185.83	245.41	184.02	264.24	181.03	251.13
DNN (HL: 9)	157.31	223.52	181.86	249.99	185.94	244.11	178.54	252.16	176.00	242.79
DNN (HL: 10)	165.88	240.03	197.50	264.04	193.75	254.01	184.72	262.70	185.54	255.43
Ours	144.79	199.57	147.52	203.86	151.31	194.65	162.75	219.76	151.66	204.72

Table 12. MAE and RMSE comparisons across day-ahead prediction models for the New-Incheon Observatory dataset (unit: kW).

Model	Jan.–Mar.		Apr.–Jun.		Jul.–Sep.		Oct.–Dec.		Avg.	
	MAE	RMSE	MAE	RMSE	MAE	RMSE	MAE	RMSE	MAE	RMSE
Persistence	115.34	172.45	149.96	228.21	145.82	205.65	115.98	175.94	131.82	196.93
Ranger	122.89	174.81	162.69	227.35	161.80	221.24	107.43	160.86	138.72	198.20
DNN (HL: 2)	131.66	190.30	169.57	237.91	173.02	234.15	111.46	169.69	146.44	210.04
DNN (HL: 3)	135.99	194.08	170.45	237.15	168.46	226.68	110.12	167.41	146.25	208.15
DNN (HL: 4)	134.87	194.99	169.32	237.75	174.55	237.38	113.04	173.29	147.96	212.70
DNN (HL: 5)	140.14	200.92	178.78	251.04	177.20	239.97	117.81	180.11	153.48	219.90
DNN (HL: 6)	136.75	195.61	172.91	243.59	173.21	232.90	112.74	171.48	148.90	212.86
DNN (HL: 7)	133.38	194.05	173.52	247.44	173.57	235.79	112.42	171.19	148.23	214.36
DNN (HL: 8)	137.65	200.24	173.35	243.62	173.48	233.39	112.83	170.10	149.33	213.79
DNN (HL: 9)	193.89	220.54	210.35	244.40	180.27	205.69	191.60	214.61	193.98	221.72
DNN (HL: 10)	141.13	204.00	184.18	259.97	181.91	245.97	120.08	183.07	156.83	225.41
Ours	119.14	158.90	150.21	196.17	142.11	179.99	97.32	135.77	127.20	169.24

Table 13. MAE and RMSE comparisons across day-ahead prediction models for the Incheon Fishery Water Purification Plant dataset (unit: kW).

Model	Jan.–Mar.		Apr.–Jun.		Jul.–Sep.		Oct.–Dec.		Avg.	
	MAE	RMSE	MAE	RMSE	MAE	RMSE	MAE	RMSE	MAE	RMSE
Persistence	161.06	234.32	154.87	234.35	154.51	214.23	131.65	198.87	150.45	220.83
Ranger	160.58	218.36	173.66	240.66	162.65	218.01	115.96	171.33	153.11	213.49
DNN (HL: 2)	177.65	243.16	196.83	270.23	176.47	233.18	127.11	187.26	169.39	235.22
DNN (HL: 3)	172.46	238.68	193.61	264.08	174.41	231.51	131.18	192.19	167.82	232.92
DNN (HL: 4)	172.92	239.06	200.84	275.78	175.70	232.54	123.82	184.64	168.20	235.11
DNN (HL: 5)	175.31	242.71	199.05	276.23	178.21	237.30	128.26	192.01	170.10	238.82
DNN (HL: 6)	174.68	241.96	200.25	277.26	177.83	234.69	126.17	189.93	169.62	237.86
DNN (HL: 7)	172.36	239.23	207.54	282.71	182.23	241.33	125.95	191.57	171.92	240.77
DNN (HL: 8)	169.13	236.70	189.34	261.31	176.14	236.41	131.86	195.42	166.54	233.56
DNN (HL: 9)	178.06	247.03	205.57	282.08	181.84	241.26	121.96	186.51	171.73	241.50
DNN (HL: 10)	180.50	248.94	197.63	276.87	175.72	233.06	125.17	187.41	169.62	238.61
Ours	159.48	215.19	160.07	213.17	151.87	191.57	108.27	153.48	144.76	194.71

Table 14. Comparative analysis of day-ahead prediction models during dry conditions and precipitation events for the New-Incheon Sonae dataset (unit: kW).

Model	Dry Conditions		Precipitation Events	
	MAE	RMSE	MAE	RMSE
Persistence	148.04	226.16	132.18	194.43
Ranger	162.22	221.27	222.66	299.37
DNN (HL: 2)	168.30	232.31	242.62	320.51
DNN (HL: 3)	162.97	224.86	233.85	311.10
DNN (HL: 4)	165.36	229.01	231.96	310.00
DNN (HL: 5)	168.15	232.02	235.51	313.18
DNN (HL: 6)	167.92	231.03	233.56	309.99
DNN (HL: 7)	164.75	228.15	231.55	309.72
DNN (HL: 8)	178.31	247.60	232.74	309.61
DNN (HL: 9)	173.04	238.68	231.76	309.26
DNN (HL: 10)	183.18	252.40	231.25	307.26
Ours	141.17	189.96	172.68	232.81

Table 15. Comparative analysis of day-ahead prediction models during dry conditions and precipitation events for the New-Incheon Observatory dataset (unit: kW).

Model	Dry Conditions		Precipitation Events	
	MAE	RMSE	MAE	RMSE
Persistence	132.09	197.70	121.07	174.92
Ranger	133.16	190.05	238.99	309.68
DNN (HL: 2)	140.60	201.77	253.37	324.57
DNN (HL: 3)	140.39	199.95	252.94	321.57
DNN (HL: 4)	142.53	205.43	246.84	316.11
DNN (HL: 5)	148.46	213.37	245.68	315.69
DNN (HL: 6)	143.37	205.17	249.96	321.25
DNN (HL: 7)	142.74	207.06	249.26	318.61
DNN (HL: 8)	144.00	206.59	247.43	316.80
DNN (HL: 9)	194.34	222.04	189.13	217.54
DNN (HL: 10)	151.89	219.14	248.70	318.62
Ours	117.37	154.93	142.40	183.84

Table 16. Comparative analysis of day-ahead prediction models during dry conditions and precipitation events for the Incheon Fishery Water Purification Plant dataset (unit: kW).

Model	Dry Conditions		Precipitation Events	
	MAE	RMSE	MAE	RMSE
Persistence	151.03	222.30	132.16	180.59
Ranger	148.93	208.00	230.29	296.06
DNN (HL: 2)	165.23	230.28	246.55	312.32
DNN (HL: 3)	164.12	228.32	238.08	305.78
DNN (HL: 4)	164.56	230.84	236.95	303.54
DNN (HL: 5)	166.36	234.68	239.89	305.54
DNN (HL: 6)	165.84	233.65	239.88	305.45
DNN (HL: 7)	167.91	236.25	245.97	312.43
DNN (HL: 8)	163.20	229.54	229.92	298.67
DNN (HL: 9)	167.80	237.19	244.91	310.70
DNN (HL: 10)	165.46	233.84	246.67	313.66
Ours	132.70	177.92	162.19	213.98

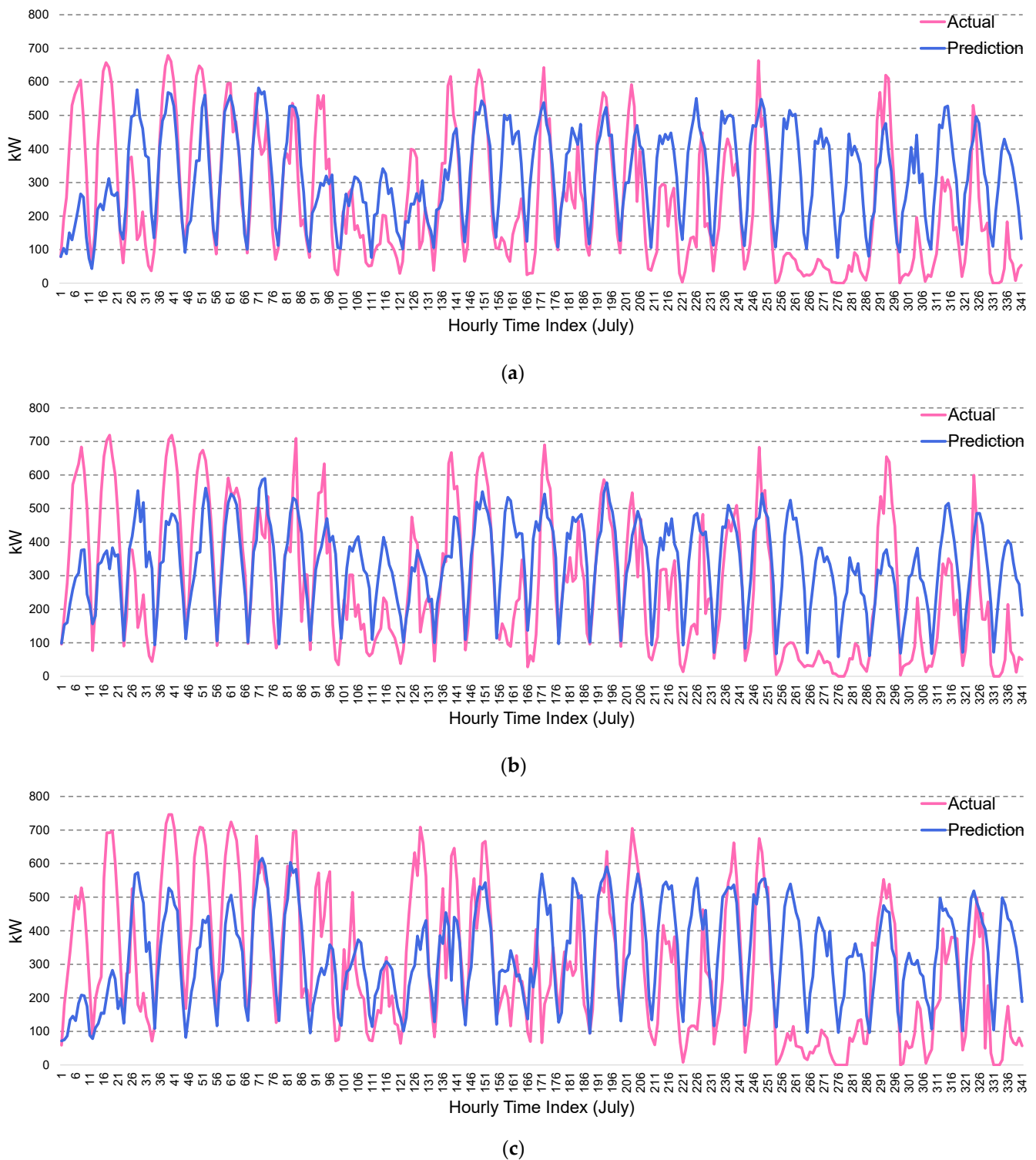


Figure 6. Comparative analysis of actual and predicted solar PV power generation for July 2019 in Incheon. (a) New-Incheon Sonae; (b) New-Incheon Observatory; (c) Incheon Fishery Water Purification Plant.

3.3. Model Interpretability

Ensuring the accuracy and trustworthiness of predictive models is paramount. As such, methods to clarify how models make decisions have gained prominence. The goal of this research was to identify the most important influencing factors in the Ranger-based online learning model. The Ranger package calculates variable importance by assessing how much

the model’s accuracy decreases when the data for each variable is shuffled. This approach quantifies the importance of each variable to the model’s predictive performance, with a higher score indicating that a variable is more important in making accurate predictions. To present these results, we used the ‘vip’ package, a notable tool in R’s extensive visualization ecosystem, to illustrate the importance of variables [74].

Figures 7 and 8 show the importance of the input variables in models with fewer hidden layers, providing an essential foundation for the detailed analysis in Figure 9. In these preliminary figures, the DNN_HL02 model, which is characterized by a lower number of hidden layers, emerges as consistently significant. This level of importance persists across different model complexities, as shown in the heatmaps. Figure 9 further illustrates that while models with a moderate number of hidden layers, specifically DNN_HL05 and DNN_HL07, show varying degrees of influence on variable importance, this does not eclipse the persistent significance of the simpler DNN_HL02 model. Such observations suggest that models of lesser complexity retain their importance alongside more complex models.

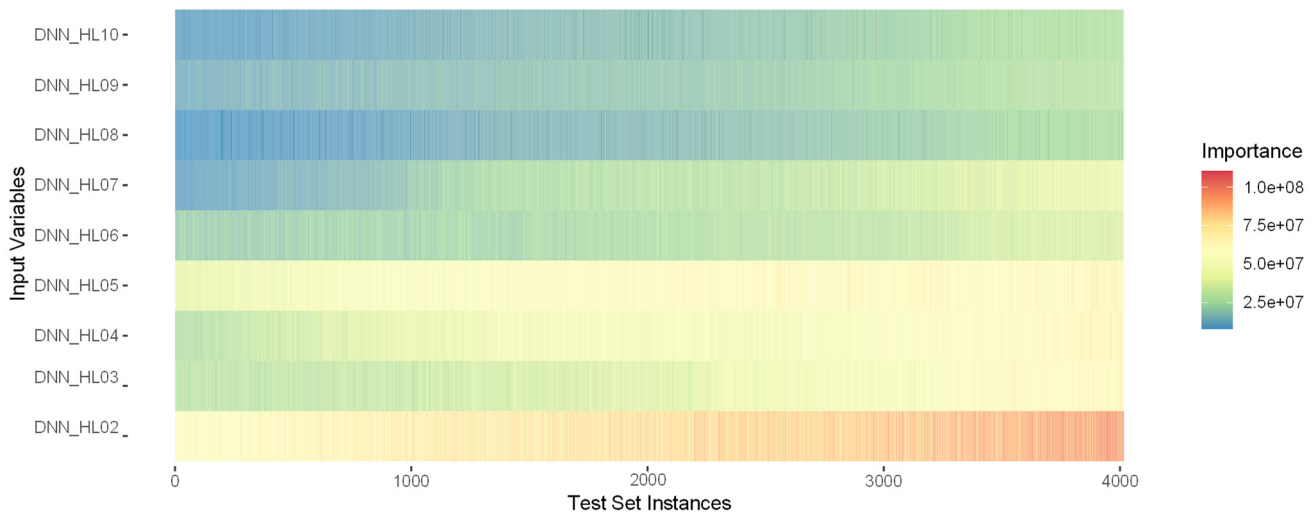


Figure 7. Variable importance heatmap of the Ranger model for New-Incheon Sonae.

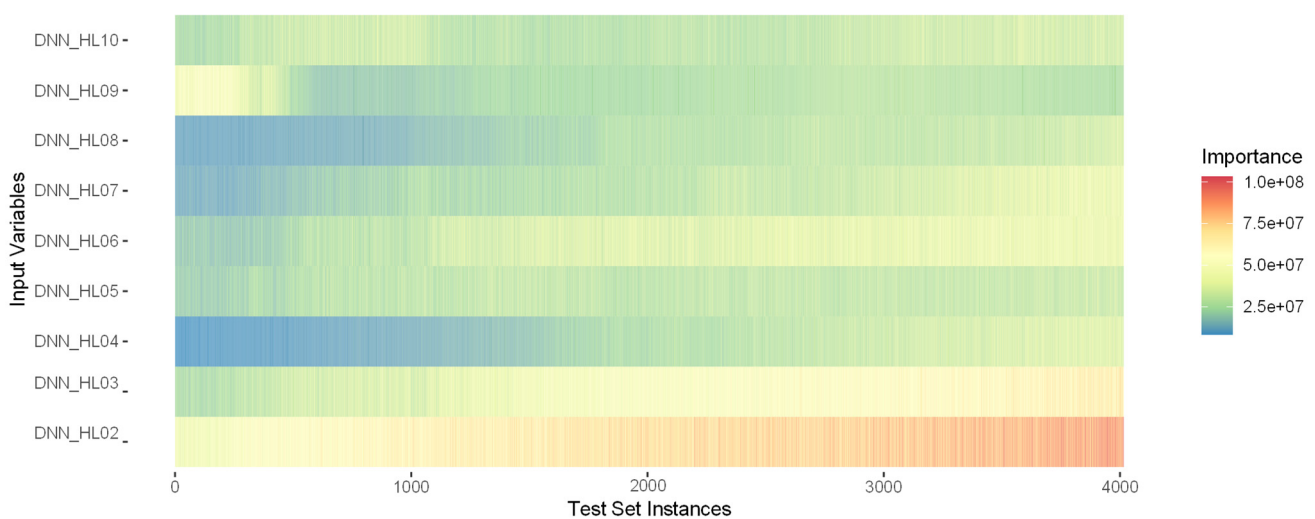


Figure 8. Variable importance heatmap of the Ranger model for New-Incheon Observatory.

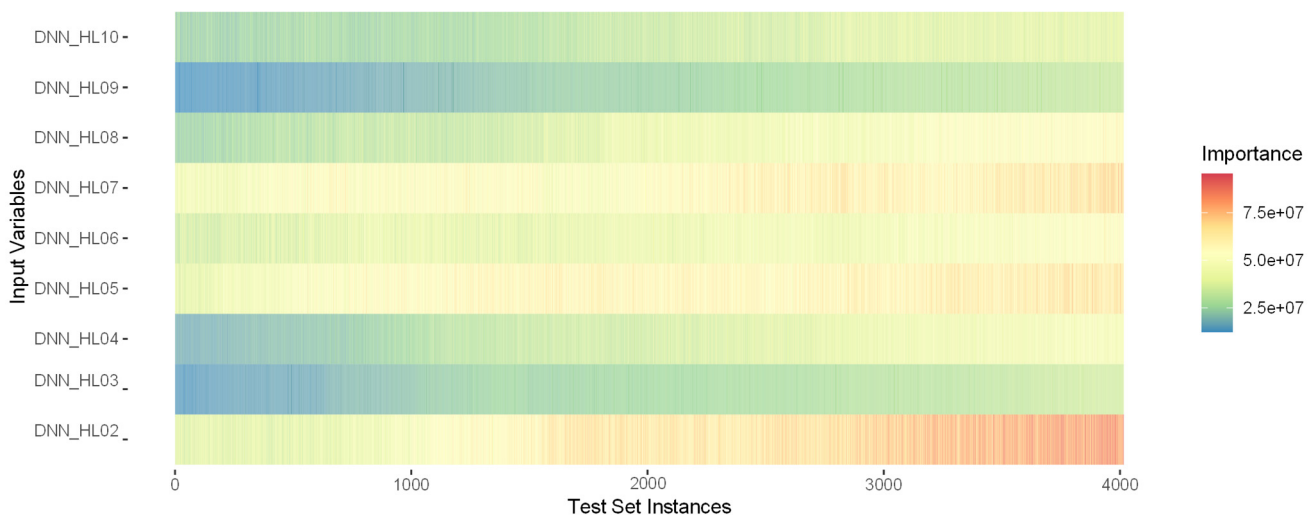


Figure 9. Variable importance heatmap of the Ranger model for Incheon Fishery Water Purification Plant.

Furthermore, DNN_HL02 not only retains its relevance across a spectrum of models but also sees an increase in its impact, suggesting an enhanced role when analyzing larger datasets. Similarly, Figure 9 shows the increasing importance of DNN_HL05 and DNN_HL07, highlighting their improved ability to decipher the complexity of the data. This reflects the complexity of the modeling process and the need to continuously explore different model frameworks to gain deeper insights. Variations observed may signal the dynamic characteristics of the subject matter at each site examined. Consistent color intensity across models indicates general agreement on key variables, while variances reveal detailed assessments of variable importance as model complexity is adjusted over time.

Our study provides an analytical view of variable importance through the lens of different DNN models, focusing on their internal evaluation rather than direct predictive performance. This calibrated view of the heatmaps provides us with a broader understanding of how different DNN configurations weigh variable importance, which aids in the strategic selection and tuning of models for the New-Incheon Sonae, New-Incheon Observatory, and Incheon Fishery Water Purification Plant datasets.

4. Discussion

In this paper, we proposed a two-stage DNN optimization method for solar PV power generation prediction. Through comparative analysis with well-known benchmark models, including Att-LSTM, Att-Bi-LSTM, Att-GRU, Att-1D-CNN, Att-TCN, Att-GRU-TCN, and Att-Bi-GRU-TCN, the proposed method highlighted the superior performance of the proposed model in terms of MAE and RMSE on three datasets: New-Incheon Sonae, New-Incheon Observatory, and Incheon Fishery Water Purification Plant. Although these results are promising, our investigation revealed limitations that guide the direction of future research to improve prediction performance.

- To address the observed forecast discrepancies under different weather conditions, we will consider incorporating additional independent variables to more accurately capture the effects of precipitation, or adopting a hybrid forecasting approach. For example, during expected rain events, we plan to leverage the predictive power of the persistence model to improve the accuracy of the proposed method.
- Solar PV power generation is strongly correlated with solar irradiation. However, none of the environmental factors used as input variables in this study were used. Therefore, in the direction of future research, it is expected that more innovative prediction performance can be developed by performing solar irradiation prediction through existing input variables and using them together as input variables.

- The hybrid models used as benchmarks are currently widely used techniques with good performance in time series forecasting. However, the training data used in this study has a period of one year, which is a very small amount of data in the field of time series forecasting, and we believe that the following performance is due to this. Therefore, if the amount of data is increased by data augmentation techniques, such as generative adversarial networks (GANs) and diffusions, the prediction performance of the models used as benchmarks will be improved, and the method proposed in this study will also be improved.
- We aim to explore the frontiers of ML techniques, including advanced DL and ensemble learning methods. These techniques have demonstrated the potential to identify complex patterns within meteorologically influenced datasets. We are optimistic that such approaches will refine the sensitivity of the proposed method to minute variations in weather patterns and, by extension, solar PV power generation.
- We will focus on the incorporation of hyper-local weather data, possibly by establishing dedicated weather monitoring stations at PV installation sites. An extension of the model's parameter set is also planned to better capture the dynamic behavior of PV systems and the nonlinear interaction of solar irradiance [75].
- Solar energy, as an important renewable energy source, is being utilized globally, but this research has been limited to the Incheon region of South Korea. Expanding our data sources to a wider range of regions will facilitate the verification of the universality of our proposed model and its ability to ensure grid stability with clean energy.

These strategic initiatives are expected to result not only in a more reliable tool for forecasting solar PV power generation but also to contribute significantly to optimizing grid management and strategic energy distribution in an era of increasingly variable renewable energy sources.

5. Conclusions

Achieving robust solar PV power generation prediction on low-performance computing systems is critical due to the need to balance cost and efficient use of computational resources. In this context, constructing the optimal DNN model for such prediction becomes a formidable challenge, requiring not only significant computational resources but also a depth of knowledge that may be beyond the reach of many energy experts. To address these issues, we proposed a stacking ensemble-based solar PV power generation prediction model that uses actual data from solar PV systems in Incheon combined with weather forecasts from the KMA. In the first stage, we constructed DNN models with 2 to 10 hidden layers using scikit-learn's MLPRegressor optimized by Optuna, which simplified the development process and ensured the accessibility of the model even on low-performance systems.

In the next phase, we focused on preparing the training dataset for our meta-regression model, a Ranger-based RF. Specifically, we used the predictions from each DNN model as input features for the meta-regression model. A key innovation was the use of fivefold cross-validation to ensure sufficient training data for our meta-regression model without the need for a separate validation set, demonstrating the effectiveness of the model despite data limitations. In addition, the Ranger-based RF online learning model effectively learns from current trends and patterns in real time, taking into account the divergence between training and evaluation periods, thereby improving prediction accuracy over time.

Experimental results demonstrated the model's superior performance in minimizing uncertainty and improving MAE and RMSE for multistep-ahead predictions. The use of RF's variable importance output clarified the contributions of different DNN models, increasing the transparency and applicability of our prediction method. Despite its strengths, the model's exclusion of solar irradiance as an input was identified as a limitation, suggesting an area for future improvement. Our study can provide robust solar PV power generation predictions on low-power systems, thus simplifying the construction of optimal DNN models for energy experts while balancing cost and computational efficiency.

Supplementary Materials: The following supporting information can be downloaded at: <https://www.mdpi.com/article/10.3390/electronics13091659/s1>, Table S1: New-Incheon Sonae_MinMax_Norm, Table S2: New-Incheon Observatory_MinMax_Norm, Table S3: Incheon Fishery Water Purification Plant_MinMax_Norm.

Author Contributions: Conceptualization, J.O. and D.S.; methodology, J.O.; software, J.O. and D.S.; validation, J.J., N.K. and J.M.; formal analysis, J.M.; investigation, D.S.; resources, J.M.; data curation, J.J. and N.K.; writing—original draft preparation, J.O. and D.S.; writing—review and editing, J.M. and E.H.; visualization, J.O. and J.M.; supervision, E.H.; project administration, E.H.; funding acquisition, J.M. and E.H. All authors have read and agreed to the published version of the manuscript.

Funding: This study was supported by BK21 FOUR (Fostering Outstanding Universities for Research) (No. 5199990514663) and the Soonchunhyang University Research Fund.

Data Availability Statement: The datasets presented in this study are publicly available in the following public repositories: The original contributions created for this study are available at the Korea Open Data Portal, accessible at <https://www.data.go.kr/index.do> (accessed on 1 October 2023), and the Korea Meteorological Administration Data Portal, accessible at <https://data.kma.go.kr/cmmn/main.do> (accessed on 1 October 2023). These resources were used in the preparation of the data supporting the findings of this study. For those interested in directly using the preprocessed datasets for model training or further analysis, the datasets have been carefully prepared and can be found in the Supplementary Material of this article, specifically in Tables S1–S3. This preparation ensures that the data are in an appropriate format for immediate use in research efforts.

Acknowledgments: We would like to express our deepest gratitude to Hwimyeong Ha of LG Energy Solution, Ltd. (Seoul, Korea). His expert insights into the nuanced considerations and specific conditions within South Korea have been invaluable in paving the way for the potential integration of our technology into photovoltaic systems. We would also like to express our sincere gratitude to the reviewers and editors for their insightful and valuable feedback, which has helped us improve our work.

Conflicts of Interest: The authors declare no conflicts of interest.

Appendix A

This section provides a comprehensive list of acronyms used throughout this document, along with their corresponding definitions. The left column lists the acronyms for quick reference, while the right column provides a detailed explanation of each term to ensure clarity and enhance the reader's understanding of the technical terminology relevant to this study:

AC	alternating current
ANN	artificial neural network
ARIMA	autoregressive integrated moving average
Att	attention mechanism
Att-1D-CNN	attention-based one-dimensional convolutional neural network
Att-Bi-GRU-TCN	attention-based bidirectional gated recurrent unit with temporal convolutional network
Att-Bi-LSTM	attention-based bidirectional long short-term memory
Att-GRU	attention-based gated recurrent unit
Att-GRU-TCN	attention-based gated recurrent unit with temporal convolutional network
Att-LSTM	attention-based long short-term memory
Att-TCN	attention-based temporal convolutional network
Bi-LSTM	bidirectional long short-term memory
CNN	convolutional neural network
CPU	central processing unit
DC	direct current
DL	deep learning
DNN	deep neural network
DT	decision tree
EV	electric vehicle

GAN	generative adversarial network
GHG	greenhouse gas
GPU	graphics processing unit
GRU	gated recurrent unit
KMA	Korea Meteorological Administration
LSTM	long short-term memory
MAE	mean absolute error
ML	machine learning
MLP	multilayer perceptron
NN	neural network
PV	photovoltaic
RF	random forest
RMSE	root mean square error
RNN	recurrent neural network
SVM	support vector machine
TCN	temporal convolutional network
TSCV	time series cross-validation
Wp	watt-peak

References

1. Olabi, A.G.; Abdelkareem, M.A. Renewable Energy and Climate Change. *Renew. Sustain. Energy Rev.* **2022**, *158*, 112111. [\[CrossRef\]](#)
2. Wang, J.; Azam, W. Natural resource scarcity, fossil fuel energy consumption, and total greenhouse gas emissions in top emitting countries. *Geosci. Front.* **2024**, *15*, 101757. [\[CrossRef\]](#)
3. Yoro, K.O.; Daramola, M.O. CO₂ Emission Sources, Greenhouse Gases, and the Global Warming Effect. In *Advances in Carbon Capture*; Woodhead Publishing: Sawston, UK, 2020; pp. 3–28.
4. Khan, Z.A.; Hussain, T.; Haq, I.U.; Ullah, F.U.M.; Baik, S.W. Towards efficient and effective renewable energy prediction via deep learning. *Energy Rep.* **2022**, *8*, 10230–10243. [\[CrossRef\]](#)
5. Wen, J.; Okolo, C.V.; Ugwuoke, I.C.; Kolani, K. Research on influencing factors of renewable energy, energy efficiency, on technological innovation. Does trade, investment and human capital development matter? *Energy Policy* **2021**, *160*, 112718. [\[CrossRef\]](#)
6. Aghaei, M.; Kumar, N.M.; Eskandari, A.; Ahmed, H.; de Oliveira, A.K.V.; Chopra, S.S. Solar PV Systems Design and Monitoring. In *Photovoltaic Solar Energy Conversion*; Academic Press: Cambridge, MA, USA, 2020; pp. 117–145.
7. Ahmad, L.; Khordehghah, N.; Malinauskaite, J.; Jouhara, H. Recent advances and applications of solar photovoltaics and thermal technologies. *Energy* **2020**, *207*, 118254. [\[CrossRef\]](#)
8. Park, S.; Kim, D.; Moon, J.; Hwang, E. Zero-Shot Photovoltaic Power Forecasting Scheme Based on a Deep Learning Model and Correlation Coefficient. *Int. J. Energy Res.* **2023**, *2023*, 1–14. [\[CrossRef\]](#)
9. Ma, W.; Chen, Z.; Zhu, Q. Ultra-Short-Term Forecasting of Photo-Voltaic Power via RBF Neural Network. *Electronics* **2020**, *9*, 1717. [\[CrossRef\]](#)
10. Ahmed, R.; Sreeram, V.; Mishra, Y.; Arif, M.D. A review and evaluation of the state-of-the-art in PV solar power forecasting: Techniques and optimization. *Renew. Sustain. Energy Rev.* **2020**, *124*, 109792. [\[CrossRef\]](#)
11. Iheanetu, K.J. Solar Photovoltaic Power Forecasting: A Review. *Sustainability* **2022**, *14*, 17005. [\[CrossRef\]](#)
12. Qazi, A.; Fayaz, H.; Wadi, A.; Raj, R.G.; Rahim, N.; Khan, W.A. The artificial neural network for solar radiation prediction and designing solar systems: A systematic literature review. *J. Clean. Prod.* **2015**, *104*, 1–12. [\[CrossRef\]](#)
13. Wang, Y.; Cao, G.; Mao, S.; Nelms, R.M. Analysis of solar generation and weather data in smart grid with simultaneous inference of nonlinear time series. In Proceedings of the IEEE INFOCOM 2015—IEEE Conference on Computer Communications Workshops (INFOCOM WKSHPs), Hong Kong, China, 26 April 2015–1 May 2015; pp. 600–605.
14. Van der Meer, D.; Mouli, G.R.C.; Mouli, G.M.E.; Elizondo, L.R.; Bauer, P. Energy Management System with PV Power Forecast to Optimally Charge EVs at the Workplace. *IEEE Trans. Ind. Inform.* **2016**, *14*, 311–320. [\[CrossRef\]](#)
15. Voyant, C.; Notton, G.; Kalogirou, S.; Nivet, M.-L.; Paoli, C.; Motte, F.; Fouilloy, A. Machine learning methods for solar radiation forecasting: A review. *Renew. Energy* **2017**, *105*, 569–582. [\[CrossRef\]](#)
16. Almonacid, F.; Fernandez, E.F.; Mellit, A.; Kalogirou, S. Review of techniques based on artificial neural networks for the electrical characterization of concentrator photovoltaic technology. *Renew. Sustain. Energy Rev.* **2017**, *75*, 938–953. [\[CrossRef\]](#)
17. Wang, Y.; Shen, Y.; Mao, S.; Cao, G.; Nelms, R.M. Adaptive Learning Hybrid Model for Solar Intensity Forecasting. *IEEE Trans. Ind. Inform.* **2018**, *14*, 1635–1645. [\[CrossRef\]](#)
18. Zhang, R.; Ma, H.; Hua, W.; Saha, T.K.; Zhou, X. Data-Driven Photovoltaic Generation Forecasting Based on a Bayesian Network With Spatial–Temporal Correlation Analysis. *IEEE Trans. Ind. Inform.* **2019**, *16*, 1635–1644. [\[CrossRef\]](#)
19. Al-Dahidi, S.; Ayadi, O.; Alrbai, M.; Adeeb, J. Ensemble Approach of Optimized Artificial Neural Networks for Solar Photovoltaic Power Prediction. *IEEE Access* **2019**, *7*, 81741–81758. [\[CrossRef\]](#)

20. Abdel-Nasser, M.; Mahmoud, K. Accurate photovoltaic power forecasting models using deep LSTM-RNN. *Neural Comput. Appl.* **2017**, *31*, 2727–2740. [CrossRef]
21. Patel, H.K. Solar Radiation Prediction Using LSTM and CNN. Ph.D. Thesis, California State University, Sacramento, CA, USA, 2021.
22. Wen, H.; Du, Y.; Chen, X.; Lim, E.; Wen, H.; Jiang, L.; Xiang, W. Deep Learning Based Multistep Solar Forecasting for PV Ramp-Rate Control Using Sky Images. *IEEE Trans. Ind. Inform.* **2020**, *17*, 1397–1406. [CrossRef]
23. Jiao, X.; Li, X.; Lin, D.; Xiao, W. A Graph Neural Network Based Deep Learning Predictor for Spatio-Temporal Group Solar Irradiance Forecasting. *IEEE Trans. Ind. Inform.* **2021**, *18*, 6142–6149. [CrossRef]
24. Zameer, A.; Jaffar, F.; Shahid, F.; Muneeb, M.; Khan, R.; Nasir, R. Short-term solar energy forecasting: Integrated computational intelligence of LSTMs and GRU. *PLoS ONE* **2023**, *18*, e0285410. [CrossRef]
25. Rocha, H.R.O.; Fiorotti, R.; Fardin, J.F.; Garcia-Pereira, H.; Bouvier, Y.E.; Rodríguez-Lorente, A.; Yahyaoui, I. Application of AI for Short-Term PV Generation Forecast. *Sensors* **2023**, *24*, 85. [CrossRef]
26. Mittal, S.; Vaishay, S. A survey of techniques for optimizing deep learning on GPUs. *J. Syst. Arch.* **2019**, *99*, 101635. [CrossRef]
27. Yang, L.; Shami, A. On hyperparameter optimization of machine learning algorithms: Theory and practice. *Neurocomputing* **2020**, *415*, 295–316. [CrossRef]
28. Moon, J.; Park, S.; Rho, S.; Hwang, E. A comparative analysis of artificial neural network architectures for building energy consumption forecasting. *Int. J. Distrib. Sens. Netw.* **2019**, *15*. [CrossRef]
29. Moon, J.; Jung, S.; Rew, J.; Rho, S.; Hwang, E. Combination of short-term load forecasting models based on a stacking ensemble approach. *Energy Build.* **2020**, *216*, 109921. [CrossRef]
30. Bâra, A.; Oprea, S. Embedding the weather prediction errors (WPE) into the photovoltaic (PV) forecasting method using deep learning. *J. Forecast.* **2024**, 1–26. [CrossRef]
31. Oprea, S.-V.; Bâra, A. On-grid and off-grid photovoltaic systems forecasting using a hybrid meta-learning method. *Knowl. Inf. Syst.* **2024**, *66*, 2575–2606. [CrossRef]
32. Oprea, S.-V.; Bâra, A. A stacked ensemble forecast for photovoltaic power plants combining deterministic and stochastic methods. *Appl. Soft Comput.* **2023**, *147*, 110781. [CrossRef]
33. Moon, J.; Park, S.; Rho, S.; Hwang, E. Robust Building Energy Consumption Forecasting Using an Online Learning Approach with R Ranger. *J. Build. Eng.* **2022**, *47*, 103851. [CrossRef]
34. Smart City Korea. Incheon-Type Smart City, Inform the World. Report; Smart City Comprehensive Portal: Smart City Korea, 2022. Available online: <https://smartcity.go.kr/en/> (accessed on 4 April 2023).
35. Wikipedia. Incheon. Available online: <https://en.wikipedia.org/wiki/Incheon> (accessed on 4 April 2023).
36. SMART CITIES INDEX REPORT. Available online: <https://smartcitiesindex.org/smartcitiesindexreport2022> (accessed on 4 April 2023).
37. Smart City Korea. Renewable Energy Business Brand Smart Energy Factory Loan Support. Report; Smart City Comprehensive Portal: SMART CITY KOREA, 2020. Available online: <https://smartcity.go.kr/en/> (accessed on 4 April 2023).
38. Korea Public Data Portal. Available online: <https://www.data.go.kr/en/index.do> (accessed on 4 April 2023).
39. Park, S.; Jung, S.; Moon, J.; Hwang, E. Explainable Photovoltaic Power Forecasting Scheme Using BiLSTM. *KIPS Trans. Softw. Data Eng.* **2022**, *11*, 339–346.
40. Yao, X.; Fu, X.; Zong, C. Short-term load forecasting method based on feature preference strategy and LightGBM-XGboost. *IEEE Access* **2022**, *10*, 75257–75268. [CrossRef]
41. Korea Meteorological Administration. KMA Weather Data Service's MET Data Portal. Available online: <https://data.kma.go.kr/resources/html/en/aowdp.html> (accessed on 4 April 2023).
42. Korea Meteorological Administration. Weather Forecast. Available online: https://www.kma.go.kr/eng/biz/forecast_01.jsp (accessed on 4 April 2023).
43. Visser, L.; AISkaif, T.; van Sark, W. Operational day-ahead solar power forecasting for aggregated PV systems with a varying spatial distribution. *Renew. Energy* **2021**, *183*, 267–282. [CrossRef]
44. Thanh, P.N.; Cho, M.Y.; Chang, C.L.; Chen, M.J. Short-term three-phase load prediction with advanced metering infrastructure data in smart solar microgrid based convolution neural network bidirectional gated recurrent unit. *IEEE Access* **2022**, *10*, 68686–68699. [CrossRef]
45. Korea Meteorological Administration. Climate Information. Available online: https://www.kma.go.kr/eng/biz/climate_01.jsp (accessed on 4 April 2023).
46. Bâra, A.; Oprea, S.-V. Machine Learning Algorithms for Power System Sign Classification and a Multivariate Stacked LSTM Model for Predicting the Electricity Imbalance Volume. *Int. J. Comput. Intell. Syst.* **2024**, *17*, 1–22. [CrossRef]
47. Kazmi, M.; Khan, H.R.; Lubaba; Bin Khalid, M.H.; Qazi, S.A. Threefold Optimized Forecasting of Electricity Consumption in Higher Education Institutions. *Comput. Mater. Contin.* **2022**, *73*, 2351–2370. [CrossRef]
48. Jang, J.; Jeong, W.; Kim, S.; Lee, B.; Lee, M.; Moon, J. RAID: Robust and Interpretable Daily Peak Load Forecasting via Multiple Deep Neural Networks and Shapley Values. *Sustainability* **2023**, *15*, 6951. [CrossRef]
49. Pedregosa, F.; Varoquaux, G.; Gramfort, A.; Michel, V.; Thirion, B.; Grisel, O.; Duchesnay, É. Scikit-Learn: Machine Learning in Python. *J. Mach. Learn. Res.* **2011**, *12*, 2825–2830.
50. Roy, S.; Mehera, R.; Pal, R.K.; Bandyopadhyay, S.K. Hyperparameter optimization for deep neural network models: A comprehensive study on methods and techniques. *Innov. Syst. Softw. Eng.* **2023**, 1–12. [CrossRef]

51. Öztürk, M.M. Initializing Hyper-Parameter Tuning with a Metaheuristic-Ensemble Method: A Case Study Using Time-Series Weather Data. *Evol. Intell.* **2023**, *16*, 1019–1031. [[CrossRef](#)]
52. Akiba, T.; Sano, S.; Yanase, T.; Ohta, T.; Koyama, M. Optuna: A Next-Generation Hyperparameter Optimization Framework. In Proceedings of the 25th ACM SIGKDD International Conference on Knowledge Discovery & Data Mining, New York, NY, USA, 25 July 2019; pp. 2623–2631.
53. Breiman, L. Random Forests. *Mach. Learn.* **2001**, *45*, 5–32. [[CrossRef](#)]
54. Bâra, A.; Oprea, S.-V.; Tudorică, B.G. From the East-European Regional Day-Ahead Markets to a Global Electricity Market. *Comput. Econ.* **2023**, 1–33. [[CrossRef](#)]
55. Tyrallis, H.; Papacharalampous, G. Variable Selection in Time Series Forecasting Using Random Forests. *Algorithms* **2017**, *10*, 114. [[CrossRef](#)]
56. Qi, Y. Random Forest for Bioinformatics. In *Ensemble Machine Learning: Methods and Applications*; Springer: New York, NY, USA, 2012; pp. 307–323.
57. Dudek, G. A Comprehensive Study of Random Forest for Short-Term Load Forecasting. *Energies* **2022**, *15*, 7547. [[CrossRef](#)]
58. Chou, J.-S.; Liu, C.-Y.; Prayogo, H.; Khasani, R.R.; Ghosh, D.; Lalitan, G.G. Predicting nominal shear capacity of reinforced concrete wall in building by metaheuristics-optimized machine learning. *J. Build. Eng.* **2022**, *61*, 105046. [[CrossRef](#)]
59. Antoniadis, A.; Lambert-Lacroix, S.; Poggi, J.-M. Random forests for global sensitivity analysis: A selective review. *Reliab. Eng. Syst. Saf.* **2020**, *206*, 107312. [[CrossRef](#)]
60. Cao, Y.; Li, H.; Yang, Y. Combining random forest and multicollinearity modeling for index tracking. *Commun. Stat.-Simul. Comput.* **2022**; 1–12. [[CrossRef](#)]
61. Leem, S.; Oh, J.; Moon, J.; Kim, M.; Rho, S. Enhancing multistep-ahead bike-sharing demand prediction with a two-stage online learning-based time-series model: Insight from Seoul. *J. Supercomput.* **2023**, *80*, 4049–4082. [[CrossRef](#)]
62. Bellahsen, A.; Dagdougui, H. Aggregated short-term load forecasting for heterogeneous buildings using machine learning with peak estimation. *Energy Build.* **2021**, *237*, 110742. [[CrossRef](#)]
63. Wright, M.N.; Ziegler, A. Ranger: A fast implementation of random forests for high dimensional data in C++ and R. *J. Stat. Softw.* **2017**, *77*, 1–17. [[CrossRef](#)]
64. Alkhamash, E.H.; Hadjouni, M.; Elshewey, A.M. A Hybrid Ensemble Stacking Model for Gender Voice Recognition Approach. *Electronics* **2022**, *11*, 1750. [[CrossRef](#)]
65. So, D.; Oh, J.; Leem, S.; Ha, H.; Moon, J. A Hybrid Ensemble Model for Solar Irradiance Forecasting: Advancing Digital Models for Smart Island Realization. *Electronics* **2023**, *12*, 2607. [[CrossRef](#)]
66. Oshiro, T.M.; Perez, P.S.; Baranauskas, J.A. How Many Trees in a Random Forest? In *Machine Learning and Data Mining in Pattern Recognition: 8th International Conference, MLDM 2012, Berlin, Germany, 13–20 July 2012*; Proceedings 8; Springer: Berlin/Heidelberg, Germany, 2012; pp. 154–168.
67. Zhou, H.; Zhang, Y.; Yang, L.; Liu, Q.; Yan, K.; Du, Y. Short-Term Photovoltaic Power Forecasting Based on Long Short Term Memory Neural Network and Attention Mechanism. *IEEE Access* **2019**, *7*, 78063–78074. [[CrossRef](#)]
68. He, B.; Ma, R.; Zhang, W.; Zhu, J.; Zhang, X. An Improved Generating Energy Prediction Method Based on Bi-LSTM and Attention Mechanism. *Electronics* **2022**, *11*, 1885. [[CrossRef](#)]
69. Jung, S.; Moon, J.; Park, S.; Hwang, E. An Attention-Based Multilayer GRU Model for Multi-Step-Ahead Short-Term Load Forecasting. *Sensors* **2021**, *21*, 1639. [[CrossRef](#)]
70. Wu, Z.; Pan, F.; Li, D.; He, H.; Zhang, T.; Yang, S. Prediction of Photovoltaic Power by the Informer Model Based on Convolutional Neural Network. *Sustainability* **2022**, *14*, 13022. [[CrossRef](#)]
71. Ren, X.; Zhang, F.; Sun, Y.; Liu, Y. A Novel Dual-Channel Temporal Convolutional Network for Photovoltaic Power Forecasting. *Energies* **2024**, *17*, 698. [[CrossRef](#)]
72. Xiao, H.; Pei, W.; Wu, L.; Ma, L.; Ma, T.; Hua, W. A novel deep learning based probabilistic power flow method for Multi-Microgrids distribution system with incomplete network information. *Appl. Energy* **2023**, *335*, 120716. [[CrossRef](#)]
73. Zhou, H.; Wang, J.; Ouyang, F.; Cui, C.; Li, X. A Two-Stage Method for Ultra-Short-Term PV Power Forecasting Based on Data-Driven. *IEEE Access* **2023**, *11*, 41175–41189. [[CrossRef](#)]
74. Greenwell, B.M.; Boehmke, B.C.; Gray, B. Variable Importance Plots—An Introduction to the vip Package. *R J.* **2020**, *12*, 343. [[CrossRef](#)]
75. Tudorică, B.-G.; Bucur, C.; Panait, M.; Oprea, S.-V.; Bâra, A. Energetic Equilibrium: Optimizing renewable and non-renewable energy sources via particle swarm optimization. *Util. Policy* **2024**, *87*, 101722. [[CrossRef](#)]

Disclaimer/Publisher’s Note: The statements, opinions and data contained in all publications are solely those of the individual author(s) and contributor(s) and not of MDPI and/or the editor(s). MDPI and/or the editor(s) disclaim responsibility for any injury to people or property resulting from any ideas, methods, instructions or products referred to in the content.